

A Multilevel Framework for Partitioning Quantum Circuits

Felix Burt^{1,2}, Kuan-Cheng Chen^{1,2}, and Kin K. Leung¹

¹Electrical and Electronics Engineering, Imperial College London, South Kensington Campus, London SW7 2AZ, UK

²Imperial Quantum Engineering, Science and Technology Centre (QuEST)

Executing quantum algorithms over distributed quantum systems requires quantum circuits to be divided into sub-circuits which communicate via entanglement-based teleportation. Naively mapping circuits to qubits over multiple quantum processing units (QPUs) results in large communication overhead, increasing both execution time and noise. This can be minimised by optimising the assignment of qubits to QPUs and the methods used for covering non-local operations. Formulations which are general enough to capture the spectrum of teleportation possibilities lead to complex problem instances which can be difficult to solve effectively. This highlights a need to exploit the wide range of heuristic techniques used in the graph partitioning literature. This paper formalises and extends existing constructions for graphical quantum circuit partitioning and designs a new objective function which captures further possibilities for non-local operations via *nested state teleportation*. We adapt the well-known Fiduccia-Mattheyses heuristic to the constraints and problem objective and explore multilevel techniques which coarsen hypergraphs and partition at multiple levels of granularity. We find that this reduces runtime and improves solution quality of standard partitioning. We place these techniques within a larger framework, through which we can extract full distributed quantum circuits including teleportation instructions. We compare the entanglement requirements and runtimes with state-of-the-art methods, finding that we can

achieve the lowest entanglement costs in most cases, while always being close to the best performing method. We achieve an average improvement of 35% over the next best performing method across a wide range of circuits. We also find that our techniques can scale to much larger circuit sizes than state-of-the-art methods, provided the number of partitions is not too large.

1 Introduction

Distributed quantum computing (DQC) is becoming an increasingly popular paradigm for building scalable quantum computers [1]. The ability to share entanglement between nodes in a network of quantum processing units (QPUs) grants access to the full quantum computational power across the network, at the expense of the additional time and noise overheads incurred by entanglement distribution [2]. Key milestones for facilitating DQC have recently been demonstrated [3, 4, 5, 6, 7, 8], while early stage experimental demonstrations have given credibility to the approach [9, 10, 11]. Despite these important achievements, there are a number of challenges faced by DQC systems that are not present in traditional, monolithic systems, which must be overcome to achieve the desired scaling. Most notably, the additional overhead introduced by entanglement distribution is significant, and can lead to very deep, slow circuits which require constant sharing of entanglement between QPUs. Estimates claim operations requiring shared entanglement are at least an order of magnitude slower than those executed on a single QPU [12]. A growing body of literature is concerned with techniques for minimising this additional overhead via optimised routines for assigning logical qubits to QPUs and covering resulting non-local operations [13, 14, 15, 16, 17,

Felix Burt: f.burt23@imperial.ac.uk

Kuan-Cheng Chen: kuan-cheng.chen17@imperial.ac.uk

Kin K. Leung: kin.leung@imperial.ac.uk

18, 19, 20, 21, 22, 23, 24, 25, 26, 27, 28, 29]. The resulting optimisation problems are typically NP-hard [30], with no polynomial-time solutions for obtaining global optima. However, similar problems have been faced and extensively explored in networking and VLSI design problems [31, 32, 33, 34, 35, 36, 37, 38, 39, 40], in which very mature, effective and efficient algorithms for partitioning graphs and circuits have been developed. This article aims to combine a number of methods and techniques employed for large-scale hypergraph partitioning and apply them to the unique case of quantum circuit partitioning. The result is a multilevel partitioning framework, inspired by state-of-the-art graph partitioners such as METIS [37], hMETIS [38] and KaHyPar [40], which exploits the particular structure of quantum circuits. The problem is broken down the problem into a number of stages, each of which is adaptive to the problem specifications. The stages are *transpilation*, *graph conversion*, *gate grouping*, *coarsening*, *partitioning*, *refinement* and *circuit extraction*. We make use of existing transpilation techniques to convert circuits into an appropriate gate set. We convert the resulting circuit to a temporally extended graph representing interaction of qubits over time. We generalise this graph to a hypergraph using a greedy algorithm for grouping gates together based on their compatibility for multi-gate teleportation, and design a cost function which captures the entanglement cost of the resulting partitioning, considering the possibility of state teleportation, gate teleportation, multi-gate teleportation and a new protocol referred to as *nested state teleportation*, in which we partially collapse gate teleportation procedures into state teleportation. We then design a variant of the Fiduccia-Mattheyses (FM) algorithm [32] which is compatible with the unique constraints of the problem and tweaked to be resistant to local minima. We then introduce the multilevel framework, investigating three different strategies for coarsening hypergraphs along the time axis, using the FM algorithm to refine the partitions at each level of granularity. We show that this improves both the efficiency of the algorithm in time, and allows us to partition with lower entanglement costs. The final stage produces a distributed quantum circuit, including all necessary instructions for teleportation of qubits and

gates between QPUs, which we demonstrate to produce equivalent output distributions to their monolithic counterparts. We demonstrate the effectiveness of the framework by comparing the entanglement costs achieved by the best of the multilevel techniques with those obtained by state-of-the-art methods in the literature. Our techniques are shown to be the most effective at reducing entanglement requirements across a wide range of circuit types, including those with high connectivity and depth, while existing methods tend to be effective in a restricted number of cases. On average, we achieve a 35% improvement in the average ratio of e-bits to two-qubit gates compared with the best benchmark method, achieved for a similar amount of computation time. Furthermore, the multilevel framework allows the complexity of the problem to be tailored to the available computational resources, thus can be applied to large-scale circuits with hundreds of qubits and gates with proper use of coarsening, provided the number of partitions is not too large (< 20).

2 Background

2.1 Distributed Quantum Computing

Distributed quantum computing (DQC) is concerned with the execution of quantum algorithms across multiple linked quantum processing units (QPUs). While this can feasibly be achieved using classical communication via circuit cutting and circuit knitting [41, 42, 43, 44, 45, 46, 47], these represent a near-term form of DQC, limited by the exponential scaling of the classical processing overhead. The alternative is entanglement-based DQC, which requires links capable of sharing purely quantum information between QPUs. This is typically implemented by optical fibres transmitting photonic qubits [48]. Qubit transmission over fibres is used to distribute pairs of entangled qubits between geographically separated locations. Shared entangled pairs are known as *e-bits* or *EPR pairs*. Two QPUs holding a shared e-bit can use local operations and classical communication (LOCC) to teleport the state of qubit which is actively involved in an algorithm from one QPU to the other [49]. This is referred to as *state teleportation*. Alternatively, the e-bit can directly moderate a non-local controlled-unitary operation [50, 51], analogously referred to as *gate teleportation*. Gate teleporta-

tion has been shown to be a flexible procedure, which can cover multiple non-local operations using the same shared e-bit [52, 51, 20].

2.2 Non-local gate coverage

Non-local gate coverage is a key target for optimisation in DQC. Any method of dividing or partitioning a quantum circuit will result in some number of non-local operations. We can formalise this by defining a set of QPUs as Q , and a set of logical qubits q . Partitioning a quantum circuit requires making an assignment $\phi : q \rightarrow Q$ mapping logical qubits to QPUs. For any two-qubit gate, defined partly by the qubits on which it operates as $g(q_i, q_j)$, the gate is non-local if $\phi(q_i) \neq \phi(q_j)$. The cost of a partitioning is thus closely related to the non-local operations present in the circuit. However, since there are many ways to cover non-local operations, the cost of a partitioning does not directly correspond to the number of non-local operations. Rather, it is a quantity which depends on the method chosen for covering non-local operations. In general, a given non-local operation can be covered in three different ways. Firstly, state teleportation can be used to teleport the state of a qubit from one QPU to another, modifying the assignment function ϕ , allowing the gate to be executed locally. Secondly, if the gate is a controlled-unitary operation, it can be executed remotely using gate teleportation, a procedure which entangles the control qubit with a communication qubit in the target QPU, then uses the linked communication qubit to control the application of the unitary. Both of these methods require a single e-bit, though state teleportation may modify the locality of future gates in the circuit. Thirdly, a non-local controlled-unitary gate may be merged into an existing gate teleportation procedure, provided certain compatibility conditions are met [20]. This has been referred to as the EJPP protocol [20], burst communication [21], extended gate teleportation [53], or simply teleportation [54]. For simplicity, we will refer to the full process of teleporting multiple gates within the same process as *multi-gate teleportation*.

2.2.1 Multi-gate teleportation

Multi-gate teleportation uses shared e-bits to provide a partially accessible clone of a particular

qubit at multiple locations, allowing certain two-qubit gates to be performed non-locally. A full multi-gate teleportation procedure can be broken up into three stages. Firstly, a qubit is entangled with a communication qubit at a distance via a shared e-bit. Following this, a series of remote operations are performed using the communication qubit as control. When all compatible gates are complete, the qubit is then disentangled from the communication qubit. The first and final steps have been referred to as the *cat-entangler* and *cat-disentangler* primitives [54], since the state of the communication qubit mirrors the state of the original qubit, a situation reminiscent of Schrodinger’s cat. For consistency with previous work, we adopt the terminology and notation introduced by Wu et al. [20], calling the multi-gate teleportation primitives the *entanglement-assisted starting and ending processes*. Mathematically, the starting and ending processes are described as linear maps on general quantum states which compose to the identity. The starting process $S_{q,e}$ maps an input state $|\psi\rangle_q$ for some root qubit q on Hilbert space \mathcal{H}_q onto a joint state between q and an auxiliary qubit e in another QPU:

$$\begin{aligned} S_{q,e}(|\psi\rangle) &= \langle 0|_q |\psi\rangle_q |0\rangle_e + \langle 1|_q |\psi\rangle_q |1\rangle_e |1\rangle_e \\ &= CX_{q,e} |\psi\rangle_q |0\rangle_e, \end{aligned} \tag{1}$$

which has the effective action of a CX gate between q and e , facilitated by the shared e-bit. The symmetry of the resulting state in Eq. 1 means that both the root qubit q and the communication qubit e behave the same when used as a control in a controlled-unitary operation. This symmetry is preserved until a non-diagonal single-qubit gate is applied to either qubit, which mixes the $|0\rangle$ and $|1\rangle$ basis components of the state. To ensure that we regain the correct state on q , the gate teleportation ending process must be applied before any gate that is not diagonal or anti-diagonal in the computational basis of the root qubit is applied [20]. The ending process, $E_{q,e}$, applied to the state $|\psi'\rangle_{q,e} = S_{q,e}(|\psi\rangle_q)$, applies the inverse map of Eq. 1:

$$\begin{aligned} E_{q,e}(|\psi'\rangle_{q,e}) \\ = Tr_e(CX_{q,e} |\psi'\rangle_{q,e} \langle \psi'|_{q,e} CX_{q,e}), \end{aligned} \tag{2}$$

where $Tr(|i\rangle\langle j|) = \delta_{i,j}$ and Tr_k is the partial

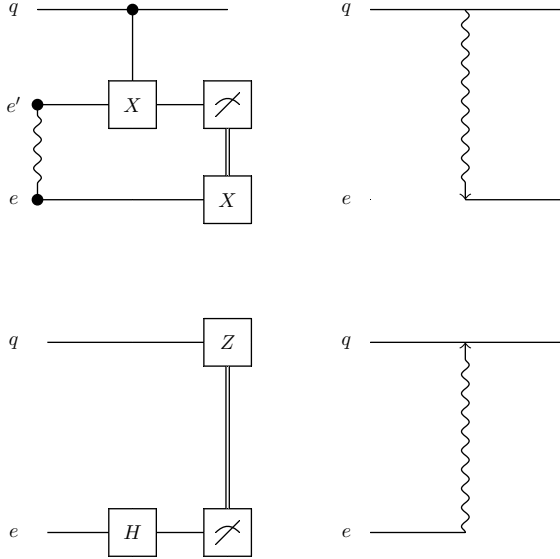


Figure 1: The starting and ending processes. The starting process $S_{q,e}$ is a linear map which maps the state of the root qubit q onto a joint state between q and an auxiliary qubit e in another QPU. The ending process $E_{q,e}$ disentangles the auxiliary qubit from the root qubit, returning the original state to q . Diagrammatic notation from Ref. [20]

trace on qubit k , which removes it from the state description. As a result, $E_{q,e} \circ S_{q,e}(|\psi\rangle_q) = |\psi\rangle_q$ [20]. If we want to perform a controlled unitary $CU_{q,q'}$, where

$$CU_{q,q'} = |0\rangle_q \langle 0|_q \otimes I_{q'} + |1\rangle_q \langle 1|_q \otimes U_{q'} = \begin{pmatrix} I_{q'} & 0 \\ 0 & U_{q'} \end{pmatrix}, \quad (3)$$

this is equivalent to performing,

$$E_{q,e} \circ CU_{e,q'} \circ S_{q,e}(|\psi\rangle_q) = CU_{q,q'} |\psi\rangle_q \quad (4)$$

If two contiguous gate teleportation processes share the same root and auxiliary qubits, q and e , then they can be merged into a single, multi-gate teleportation procedure, which uses the same starting and ending processes. As described in Ref. [55], this can be straightforwardly generalised to link multiple QPUs. A k -fold starting process $S_{q,\mathbb{E}}$ rooted on q acting on a set of auxiliary qubits \mathbb{E} spanning k QPUs, can be described as:

$$\begin{aligned} S_{q,\mathbb{E}}(|\psi\rangle) &= \langle 0|_q |\psi\rangle_q |0\rangle_q \bigotimes_{e \in \mathbb{E}} |0\rangle_e \\ &+ \langle 1|_q |\psi\rangle_q |1\rangle_q \bigotimes_{e \in \mathbb{E}} |1\rangle_e \quad (5) \\ &= \prod_{e \in \mathbb{E}} CX_{q,e} |\psi\rangle_q \bigotimes_{e \in \mathbb{E}} |0\rangle_e. \end{aligned}$$

Without any network constraints, n e-bits allows n QPUs to be linked to the root qubit q . Once the link state is active, it can be used to control any number of contiguous controlled-unitary operations in each linked QPU via merging the teleportation procedures:

$$\begin{aligned} \prod_{q' \in \mathbb{Q}} U_{q,q'} |\Psi\rangle &= E_{q,\mathbb{E}} \circ \left(\prod_{q',e \in \mathbb{Q} \times \mathbb{E}} (U_q \otimes I_e \otimes U_{q'}) (I_q \otimes CU_{e,q'}) \right) \circ S_{q,\mathbb{E}}(|\Psi\rangle), \quad (6) \end{aligned}$$

where $|\Psi\rangle$ is the state across the full Hilbert space of the root qubit q and all $q' \in \mathbb{Q}$, which are the *receivers* in the gate teleportation. The starting and ending processes, however, still act only on the subspace of the root qubit and the auxiliary qubits. A *compatible* two-qubit unitary is given by

$$\prod_{q' \in \mathbb{Q}} U_{q,q'} = \prod_{q',e \in \mathbb{Q} \times \mathbb{E}} (U_q \otimes U_{q'}) CU_{q,q'}, \quad (7)$$

for $\theta = 2n\pi$ (diagonal) or $\theta = (2n+1)\pi$ (anti-diagonal) in the general single-qubit unitary $U(\theta, \phi, \lambda)$ 14 on q . In the anti-diagonal case, $U_e = X_e$ is applied to account for the flipping of the basis components caused by U_q . Otherwise, $U_e = I_e$. Eq. 7 omits single-qubit and two-qubit gates acting on qubits in \mathbb{Q} which are independent of the root qubit q , since there are no restrictions on such gates for multi-gate teleportation. Fig. ?? contrasts the coverage of a non-local operation using the starting and ending processes with a state teleportation procedure.

An important point to note is that the most effective method for covering non-local operations depends highly on the structure of the circuit, and the choice of method can have a significant impact on the resulting entanglement cost, quantified by the number of e-bits required. For example, methods which depend entirely on state teleportation, such as the fine-grained partitioning approach of Baker et al. [23], are very effective for quantum volume and arithmetic circuits,

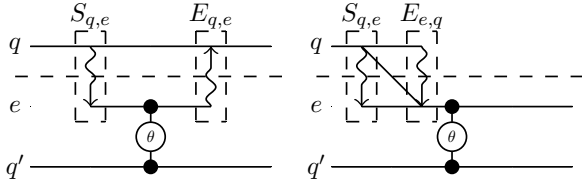


Figure 2: Methods for covering a non-local operation. On the left is the entanglement-assisted starting and ending processes $S_{q,e}$ and $E_{q,e}$, used for a gate teleportation. On the right, we flip the direction of the ending process to $E_{e,q}$, which allows us to teleport the state of q onto e .

while they tend to be less effective for circuits with more erratic connectivity and high potential for multi-gate teleportation [53, 23]. Alternatively, multi-gate teleportation methods are effective for circuits densely packed with two-qubit gates, since many opportunities arise for merging teleportation procedures together [55].

2.2.2 Nested state teleportation

We note an interesting feature of the above formulation of gate teleportation – the starting process and the ending process are identical to those used in state teleportation, except the indices for the ending process are flipped. Accordingly, we may define a state teleportation procedure from q to e as:

$$E_{e,q} \circ S_{q,e}(|\psi\rangle_q) = |\psi\rangle_e, \quad (8)$$

where we have exchanged the indices q and e , meaning that q is measured, and the classically controlled operation is applied, such that the state of q is teleported onto e . In Fig. 2, we use the same diagrammatic notation to indicate a state teleportation built out of the starting and ending processes. What is interesting about this is that it indicates we may always collapse a gate teleportation procedure into a state teleportation by redirecting the ending process. If we perform a k -fold starting process $S_{q,\mathbb{E}}$ on q and a set of auxiliary qubits \mathbb{E} , we create the state in Eq. 5. To collapse the state onto \tilde{e} we perform the following

$$E_{\tilde{e},\mathbb{E}} \circ S_{q,\mathbb{E}}(|\psi\rangle_q), \quad (9)$$

where $\tilde{\mathbb{E}} := (\mathbb{E} \setminus \tilde{e}) \cup \{q\}$, such that we replace q with \tilde{e} in ending processes for all other auxiliary qubits, and interchange q and \tilde{e} for the ending

process corresponding to $S_{q,\tilde{e}}$. In Fig. 3, we illustrate a situation where this is of use. We perform a 2-fold starting process rooted on q_1 , located in QPU B , using auxiliary qubits in A and C , allowing us to execute $CP(\theta)$ gates with q_0 and q_3 , as well as the local gate with q_2 . The H gate on q_1 requires us to end the gate teleportation. Since we have a further gate between q_1 and q_3 , we choose to re-route all ending processes towards C , collapsing the final state onto the auxiliary qubit in C . In fact, for each ending process, we may route the ending process to any QPU which still has an active link, provided the final ending process ends up at our chosen destination. We refer to this as *nested state teleportation*, since we are effectively nesting a state teleportation inside a k -fold multi-gate teleportation process.

2.3 Generalised Circuit Partitioning

The generalised circuit partitioning (GCP) was introduced in Burt et al. [53], with the aim of creating an optimisation framework which unifies multi-gate and state teleportation methods when partitioning quantum circuits. Here we recap the basics of the framework and provide some extensions and clarifications on the notation. GCP uses a graphical picture of quantum circuits, with a spatial and a temporal component, which is extended to a hyper-graph construction. Consider a circuit C , which consists of d sets of gates $g^{(t)}$, corresponding to each independent time step t of the circuit. Each $g^{(t)}$ contains the single and two-qubit gates for time step t of the circuit, where each gate is defined by its parameters and the qubits on which it acts, which are elements of the set of logical qubits Q_L .

The graph, $H(V, E)$, consists of $n_q d$ nodes, where each qubit i maps to d nodes, where $v_i^{(t)}$ is a node representing qubit i at the t^{th} time-step of the circuit and d is the total depth of the circuit, including initialisation and measurement. The total set of nodes V can be considered as the union of d subsets $V^{(t)}$ of nodes

$$V = \bigcup_{t=0}^{d-1} V^{(t)}, V^{(t)} = \{v_i^{(t)} : \forall i \in Q_L\}. \quad (10)$$

The set of edges can be considered to be the union of two separate sets, the state edges E_s and the gate edges E_g .

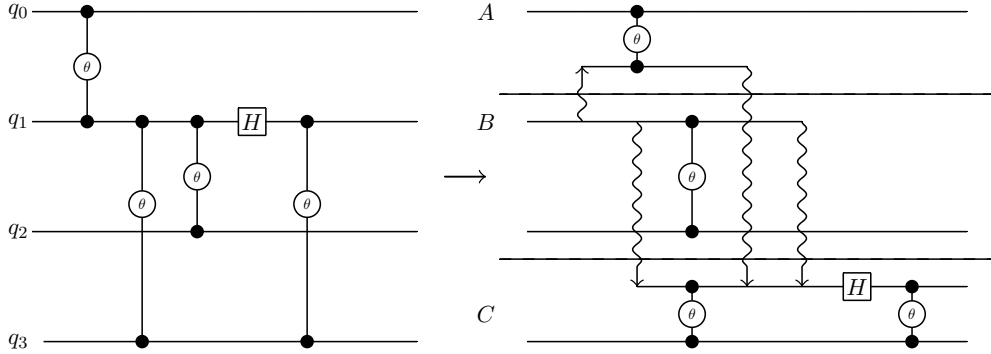


Figure 3: The nested state teleportation procedure. A 2-fold starting process is applied to link q_1 to QPUs A and B . After executing non-local gates, the starting processes are converted to a state teleportation from B to C by re-routing the ending processes towards C .

$$E = E_s \cup E_g, \quad (11)$$

$$E_s = \{(v_i^{(t)}, v_i^{(t+1)}) : \forall i \in Q_L, \forall t \in \{0, 1, \dots, d-1\}\} \quad (12)$$

$$E_g = \{(v_i^{(t)}, v_j^{(t)}) : (i, j) \in g^{(t)}, \forall t \in \{0, 1, \dots, d-1\}\} \quad (13)$$

For simplicity, the graph is built using a general gate set consisting of the following two gates:

$$U(\theta, \phi, \lambda) = \begin{pmatrix} \cos(\theta/2) & -e^{i\lambda} \sin(\theta/2) \\ e^{i(\phi+\lambda)} \sin(\theta/2) & e^{i\phi} \cos(\theta/2) \end{pmatrix} \quad (14)$$

$$CP(\theta) = \begin{pmatrix} 1 & 0 & 0 & 0 \\ 0 & 1 & 0 & 0 \\ 0 & 0 & 1 & 0 \\ 0 & 0 & 0 & e^{i\theta} \end{pmatrix}. \quad (15)$$

The gate set has a number of advantages. It allows us to compress many single-qubit gates together into one single U , while also allowing us to identify gates only by their respective parameters (three for each single-qubit gate and one for each two-qubit gate). Single-qubit gate parameters can be stored as node attributes while the two-qubit gate parameters can be stored as edge attributes. Furthermore, the $CP(\theta)$ gate is symmetric, which means both qubits can play the role of the root in a gate teleportation procedure [56]. In contrast, for a CX gate, only the control qubit can be the root. This allows for many more gate grouping possibilities.

An example of the graph at this stage is shown in Fig. 4a. At this stage, partitioning the nodes

corresponds to choosing a set of state and gate teleportation operations to cover the non-local gates in the circuit, where each *cut* edge indicates the use of an e-bit. A cut state-edge corresponds to state teleportation, and a cut gate-edge to gate teleportation (see Fig. 4b). However, we would like to consider opportunities for multi-gate teleportation. Typically, circuit partitioning methods choose to allocate qubits before merging teleportation procedures [57, 20, 21]. An exception to this is the original hypergraph partitioning strategy of Andres-Martinez and Heunen [56], which is also used in Ref. [55], which considers all possible combinations of gate groups when partitioning. Since we would like to partition qubits over time, but also consider multi-gate teleportation, we group gates in advance of partitioning, by choosing a subset of all possible gate groups which are merged into hyper-edges before partitioning. Grouped gates may end up as local or non-local after the partitioning. Thus, we partition the graph with prior knowledge of how gates will be grouped together if they are non-local, allowing us to efficiently determine the resulting e-bit cost. The limitation of this is that we must choose a strategy for grouping gates beforehand, which may turn out to be sub-optimal for the resulting partitions. We conjecture that this is still more effective than the reverse procedure, in which we choose the partition first, which may turn out to be sub-optimal for the best resulting set of gate teleportations. In order to ensure that the partitioning objective directly corresponds to the e-bit cost, we will need to design a unique cost function for the problem (see Eq. 18).

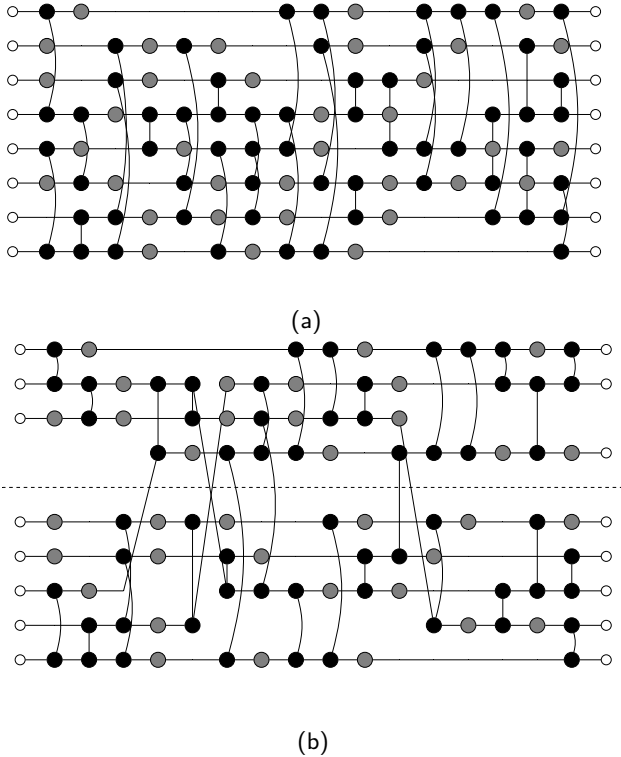


Figure 4: Base graph for a random, 8-qubit circuit. Figure 4a shows the unpartitioned graph, while Figure 4b shows the same graph with an optimised partitioning.

Gate grouping

Gate grouping requires conditions for teleportation compatibility, as described in Sec. 2.2, as well as a rule for choosing which gates should be added to which groups where there are multiple available. Multiple gates can be considered a teleportation compatible group if

1. Two-qubit gates share a common control qubit.
2. Gates are contiguous on the common control qubit.
3. Single qubit gates on the common control are *diagonal* or *anti-diagonal*.

The common control qubit is assigned as the “root” qubit of the group, while the other qubits are assigned as “receiver” qubits. Recall that, since $CP(\theta)$ gates are symmetric, both qubits can be considered to be a control, making gate teleportation possible in both directions. This means that either qubit can serve as the root. However, once we have assigned an edge to a group as a receiver, we do not consider other possible groups rooted on that edge. To define the

groups, we use the routine described in Alg. 1. In essence, the algorithm works by scanning the graph from time-step $t = 0$ to d , identifying potential merges, and adding identified gates to the largest existing group with which it is compatible. When encountering an incompatible single-qubit gate (non-diagonal) on the root of a group, the corresponding group must be closed. For each identified group, we replace all gate edges with hyper-edge object identified by the *root control* node (i.e., the node $v_i^{(t)}$, where t is the time-step of the first gate in the group). The hyper-edge, in this case, is defined by two sets of nodes referred to as the *root set* and the *receiver set*.

Formally, for each edge

$$e = e_{root} \cup e_{rec}, \quad (16)$$

where $e_{root}, e_{rec} \subset V$.

The root set contains each node associated with the root qubit from the time step of the first gate in the group to the time step of the last gate in the group, while the receiver set consists of all gate-like edges stemming from the root control node. Defined this way $|e_{root}| \geq |e_{rec}|$ for all groups, since the partition assignment of the root at each time-step may effect the cost of the group, while for the receivers we are only concerned with the assignment at the time-step of the gate. The grouping algorithm is shown in Alg. 1.

The definition of the group in terms of the root and receiver set provides a simple mechanism for calculating the cost of a partitioned hyper-edge, despite the fact that the nodes represent different points in time. To see this we must first define an assignment function $\Phi : V \rightarrow Q$ mapping nodes to the set of QPUs, thus partitioning the nodes into disjoint subsets which, for the i^{th} QPU, we may call P_i . The cost of each hyper-edge must correspond to the entanglement cost associated with covering all gates in the group given the assignment of the qubits. If the root qubit remains in its starting QPU for the duration of the group, then this corresponds to the standard hyper-cut, given by one less than the number of partitions spanned by the hyper-edge. However, if a state edge between two nodes in the root set is cut, this indicates a nested state teleportation. For each partition k which appears in the set $\{\Phi(v) : v \in e_{rec}\}$, a starting process must be performed. However, for each partition in $\{\Phi(u) : u \in e_{root}\}$, we have a corresponding

Algorithm 1: GREEDYGROUPING

Input: A hypergraph $H = (V, E)$ where each node v corresponds to qubit q_v at time $t_v \leq d$.

Output: A new hypergraph H' in which teleportation-compatible groups are merged into hyper-edges.

$H' \leftarrow H$;

GROUPS $\leftarrow \{\}$; // Dictionary keyed by qubits; each entry has rootSet and recSet

for $t' \leftarrow 0$ to $d - 1$ do

$V'_{t'} \leftarrow \{v \in V \mid t_v = t'\}$;

 foreach $v \in V'_{t'}$ do

$(\theta_v, \phi_v, \lambda_v) \leftarrow v.params$;

 if there is a gate-edge $e = (u, v) \in E$ then // This node is in a 2-qubit gate

 remove e from E ;

 if $q_v \in GROUPS$ and $q_u \notin GROUPS$ then

 GROUPS[q_v].recSet \leftarrow GROUPS[q_v].recSet $\cup \{u\}$;

 else if $q_u \in GROUPS$ and $q_v \notin GROUPS$ then

 GROUPS[q_u].recSet \leftarrow GROUPS[q_u].recSet $\cup \{v\}$;

 else if $q_v \in GROUPS$ and $q_u \in GROUPS$ then

$w \leftarrow LARGESTGROUP(q_u, q_v)$; // pick whichever group is bigger or unify

 GROUPS[w].recSet \leftarrow GROUPS[w].recSet $\cup \{u, v\}$;

 else

 GROUPS[q_u] $\leftarrow (\{\}, \{v\})$; // rootSet, recSet

 GROUPS[q_v] $\leftarrow (\{\}, \{u\})$; // two new prospective groups

 else // Single-qubit or idle

 if $\theta_v = n\pi$ then // Check if gate is diagonal/anti-diagonal

 // Group can continue

 else

 if $q_v \in GROUPS$ then

 rootSet \leftarrow GROUPS[q_v].rootSet;

 recSet \leftarrow GROUPS[q_v].recSet;

$e' \leftarrow (rootSet, recSet)$;

 add e' to E' ;

 GROUPS.pop(q_v); // Remove group for q_v

return H' ;

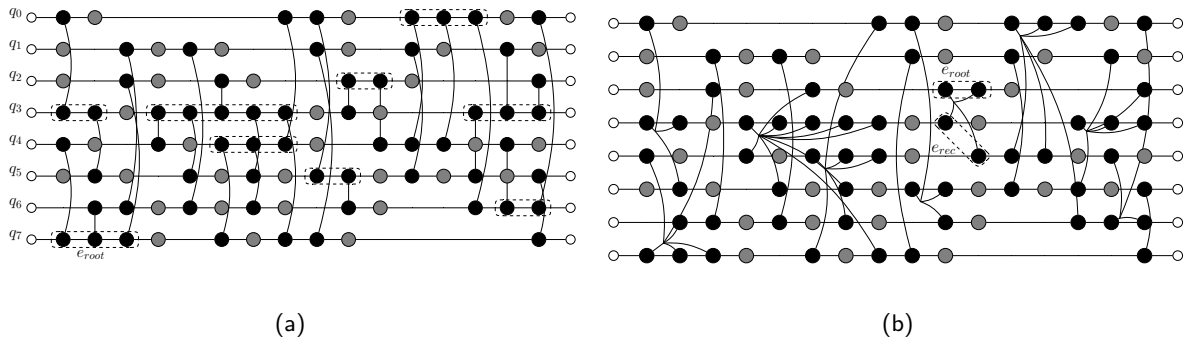


Figure 5: Illustration of grouping gate edges into hyper-edges. Fig. 5a shows the root sets identified using Alg. 1. The root set is the set of nodes corresponding to the root qubit of the group, i.e. the qubit which will be linked to receiving QPUs via cat-entanglement. Fig. 5b shows the resulting hyper-edges after grouping. Each hyper-edge contains a root set and a receiver set.

ending process routed to $\Phi(u)$ which collapses the starting process to $\Phi(u)$. If we have only one partition in the root set, then we simply collapse the state back to the root qubit at the end of the group, completing a standard multi-gate teleportation. However, for each additional partition in the root set, we collapse the state by re-routing the ending process to this partition. The e-bit cost is thus accounted for by the cut state-edge, rather than the hyper-edge. When the group is complete, the state of the root qubit will be located at $\Phi(u')$, where u' corresponds to the final root node in the group. This allows us to define the hyper-edge cost as the length of the set of partitions in the receiver set which are not present in the root set, i.e. the number of partitions which are not accounted for by nested state teleportation. We write this as

$$c_e(\Phi) = |\{\Phi(v) : v \in e_{rec}\} / \{\Phi(u) : u \in e_{root}\}|, \quad (17)$$

Since the standard state and gate edges are special cases of hyper-edges where the distinction between root and receiver sets is arbitrary, we define all edges this way, ensuring that state and gate edges contain one node in each of the root and receiver sets. This allows us to define the partitioning objective

$$\min_{\Phi} \sum_{e \in E} c_e(\Phi), \quad (18)$$

which we refer to as the *entanglement cost*, since it is designed to correspond to the number of e-bits required to partition the circuit. Eq. 18 can be written in a number of different forms – the

form presented is appropriate under the assumption of all-to-all connectivity. In the case of limited connectivity, the cost function must be decomposed such that each contribution is scaled by a path dependent function, which depends on the auxiliary entanglement requirements for entanglement swapping and purification. We restrict to all-to-all connectivity as a base for demonstrating the capability of the framework. The constraints on Φ are determined by the qubit capacity of the QPUs. Since we have a set of nodes for each time-step, we can define the partitions as subsets of each $V^{(t)}$, such that we have separate partitions $P_i^{(t)}$ for each time-step t . This allows us to define particular balance constraints according to the data qubit capacity of each QPU, which cannot be exceeded at any time-step of the circuit.

$$|P_i^{(t)}| \leq |Q_i|, \forall i \in \{0, 1, \dots, K-1\}, \forall t \in \{0, 1, \dots, d-1\}, \quad (19)$$

where $K = |Q|$ is the number of QPUs, corresponding to the number of partitions.

2.4 Fiduccia-Mattheyses

The Fiduccia-Mattheyses algorithm is an efficient, widely studied graph partitioning heuristic [32], which has a time complexity that is linear in the number of nodes and can effectively handle more complex structures such as hypergraphs. The algorithm leverages efficient data structures for storing and updating the net cost of moving nodes between partitions, avoiding redundant calculations. Balance constraints can be straightforwardly enforced by avoiding moves that violate the conditions or using a tolerance. Given an ini-

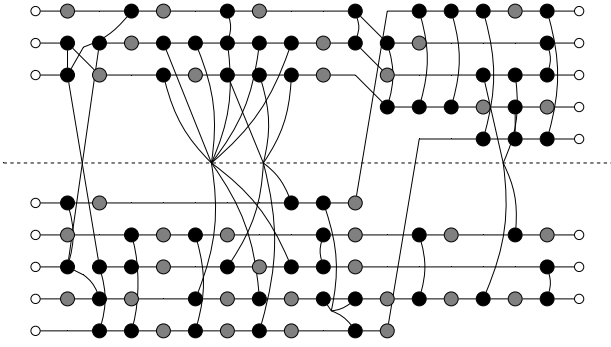


Figure 6: Graph from Fig. 5b after partitioning. For visual clarity, we return all local contributions to hyper-edges to their original gate edges, such that only non-trivial hyper-edges are shown. Note that some hyper-edge contributions which still appear to be local indicate that there has been a nested state teleportation. A gate teleportation procedure is started and then converted to a state teleportation after the final gate in the group.

tial bi-partitioning of the nodes, a single pass of the algorithm is executed as follows:

1. Calculate the cost of moving each node to the other partition.
2. Sort all moves into *gain buckets*, where each bucket contains all moves resulting in a particular gain or loss in total cost.
3. Choose a node from the highest gain bucket and move it to the other partition.
4. Remove the chosen node from the bucket and update the gains of all neighbouring nodes, moving them to their new buckets.
5. Repeat steps (4-5) until no nodes are left in the bucket.
6. Roll back to the partitioning at the iteration of maximum net gain.

The pass is repeatedly executed up until no gain is achieved or a pass limit is reached. Note that, since our aim is to minimise the cut, positive gain corresponds to reduction in the total cut. Storing the gains of all node exchanges and only updating the neighbours results in a time complexity $\mathcal{O}(n)$ which is linear in the number of nodes n , provided the gain updates are performed in constant time. This relies on the number of neighbours of each node being bounded by a constant. When dealing with problems requiring k partitions, the algorithm can be modified

by calculating gains for moving each node to each external partition, such that the number of node exchanges queried increases from n to $n(k-1)$, resulting in a time complexity $\mathcal{O}(kn)$.

3 Quantum Circuit Partitioning with Fiduccia-Mattheyses

The natural extension of FM to hypergraphs, as well as the ease of enforcing balance constraints, make it a strong candidate to be adapted for the temporal hypergraph construction. The fundamental differences between the quantum circuit case and standard balanced min-cut graph partitioning lie in the balance constraints and the objective. In particular, graphs from quantum circuits give balance constraints which are defined by the data qubit capacity of each QPU, which must be satisfied for each time step of the circuit, resulting in d separate balance constraints for a given graph. Additionally, the cost function for quantum circuits is designed to minimise e-bit use, which means the cost of moving nodes must be defined by how it affects Eq. 18. The result is that, while the structure of the algorithm remains primarily the same, new conditions must be defined for enforcing the balance and the calculation of the cost of node moves must be handled differently. First we define $A(v)$ as the adjacency set of node v , containing all edges and hyper-edges in which v is present. Contrast with the set of neighbouring nodes, $N(v)$, which is the set of all nodes present in the edges in $A(v)$. Each edge in $A(v)$ has a contribution to the cost under assignment $\Phi(v)$. When a node is moved, $\Phi(v)$ updates to $\Phi(v)'$. The change in cost for each e in $A(v)$ can be calculated simply as

$$\delta_e(\Phi, \Phi') = c_e(\Phi') - c_e(\Phi). \quad (20)$$

We refer to this as the *gain contribution* from e . The total *gain* of moving node v

$$g_v(\Phi, \Phi') = \sum_{e \in A(v)} \delta_e(\Phi, \Phi'). \quad (21)$$

Equally important is the change in gain after a particular node has been moved, since this must be computed for all neighbours $N(v)$ of moved node v after the action is taken. This is referred to as the delta gain, $\Delta g_{u,v}$, for node u from moving node v . In order to retain the $\mathcal{O}(kn)$ time

Algorithm 2: Fiduccia–Mattheyses for Temporal Hypergraphs

Input: $H = (V, E)$: Temporal hypergraph
 K : number of partitions (QPUs)
 Φ : initial assignment ($\Phi : V \rightarrow \{0, \dots, K - 1\}$)
Capacity[k]: max qubit capacity in each partition k
COSTS: precomputed cost table for hyperedge configurations
 L : total number of passes
Output: Updated partition assignment $\tilde{\Phi}$ with reduced entanglement cost.

```
 $\tilde{\Phi} \leftarrow \Phi$   
 $bestCost \leftarrow \text{COST}(H, \Phi, \text{COSTS})$   
for  $pass \leftarrow 1$  to  $L$  do // Repeat for  $L$  passes  
   $LOCK \leftarrow \emptyset$   
   $GAINS \leftarrow \text{COMPUTEALLGAINS}(H, \Phi, K, \text{COSTS})$   
   $BUCKETS \leftarrow \text{BUILDGAINBUCKETS}(GAINS)$  // Initialise gain structure  
   $cumGain \leftarrow 0$   
   $GAINLIST \leftarrow [0]$   
   $ASSIGNLIST \leftarrow [\Phi]$   
  while  $|LOCK| < |V|$  do  
     $(v^*, p^*) \leftarrow \text{BESTMOVE}(BUCKETS, LOCK, \text{Capacity}, \Phi)$   
    if  $(v^*, p^*) = \text{None}$  then  
      break // No valid moves remain this pass  
     $gain \leftarrow GAINS[v^*, p^*]$   
     $cumGain \leftarrow cumGain + gain$   
     $\Phi \leftarrow \text{MOVENODE}(\Phi, v^*, p^*)$   
     $GAINLIST.append(cumGain)$   
     $ASSIGNLIST.append(\Phi)$   
     $LOCK \leftarrow LOCK \cup \{v^*\}$   
     $\text{UPDATEGAINS}(H, GAINS, BUCKETS, v^*, p^*, \Phi, \text{COSTS})$  // Update gain structure  
  // Roll back to the best iteration in this pass  
   $bestIter \leftarrow \arg \min(GAINLIST)$   
   $\Phi \leftarrow ASSIGNLIST[bestIter]$   
  if  $\text{COST}(H, \Phi, \text{COSTS}) < bestCost$  then  
     $\tilde{\Phi} \leftarrow \Phi$   
     $bestCost \leftarrow \text{COST}(H, \Phi, \text{COSTS})$   
return  $\tilde{\Phi}$ 
```

complexity of FM, the delta gain must be computed in constant time, and should avoid recomputing any auxiliary values where possible. To do this, we pre-compute the cost of all possible configurations of a hyper-edge. Following the approach of Huang and Khang [36], we denote the *configuration* of a set of nodes A assigned to partitions by Φ as a binary string of length $K = |Q|$:

$$cf g_i^{(A)}(\Phi) = \begin{cases} 1 & \text{if } \exists v \in A : \Phi(v) = i \\ 0 & \text{otherwise} \end{cases} \quad (22)$$

where a 1 at element i indicates the presence of at least one node in P_i . Many different assignments may map to the same configuration, though the cost is completely determined by the configuration. Since we are interested in the e-bit count for each hyper-edge, we use the configurations of the root and receiver set to define the overall configuration of the edge. For each partition i , the configuration must give 1 if there is at least one receiver node in i and no root node in i . We can define this using the bitwise expression:

$$cf g_i^{(e)}(\Phi) = cf g_i^{(e_{rec})}(\Phi) \wedge \neg cf g_i^{(e_{root})}(\Phi). \quad (23)$$

The associated cost is the bit-count, i.e., the number of ones, in the final configuration. There are $2^K - 1$ possible configurations, and each configuration string identifies with an integer between 0 and $2^K - 1$. The cost of each configuration $c_e(\Phi)$ can be pre-computed and stored at the associated index of a vector C , such that it can be called in $\mathcal{O}(1)$ time. This is feasible for moderately sized K (≤ 25) architectures, though for future large scale-systems this may not be possible. In order to efficiently calculate the delta gain, we need to store the configuration of the edge and determine the change in configuration after an action is made. Since any node move has a unique source and destination, finding the new configuration requires changing a maximum of two elements of the configuration, so can be done in constant time. The nature of the gate grouping routine results in each node being part of at most *four* edges, since each node is part of at most two state edges and two gate edges. This is because a root node in a particular group may be part of the receiver set of another group. In this case, each node can be involved in a maximum of four edges and a minimum of one edge (note that, when the multilevel framework is introduced in

Sec. 4, this will not be the case). With this restriction, calculating $\Delta g_{u,v}(\Phi, \Phi', \tilde{\Phi}, \tilde{\Phi}')$ requires calculating the contribution from each edge adjacent to u , each of which requires *at most* four configurations [36] for each edge, giving a maximum of 16 configurations. To see this, consider node v being moved from P_i to P_j , updating Φ to Φ' . Before the move, the action of moving node u from P_k to P_l is $g_u(\Phi, \tilde{\Phi})$. The delta gain must obey

$$g_u(\Phi', \tilde{\Phi}') = g_u(\Phi, \tilde{\Phi}) + \Delta g_{u,v}(\Phi, \Phi', \tilde{\Phi}, \tilde{\Phi}'), \quad (24)$$

where $\tilde{\Phi}'$ corresponds to the assignment after both moves have been made. Eq. 24 implies

$$\Delta g_{u,v}(\Phi, \Phi', \tilde{\Phi}, \tilde{\Phi}') = g_u(\Phi', \tilde{\Phi}') - g_u(\Phi, \tilde{\Phi}) \quad (25)$$

$$= \sum_{e \in A(u) \cap A(v)} [\delta_e(\Phi', \tilde{\Phi}') - \delta_e(\Phi, \tilde{\Phi})] \quad (26)$$

$$= \sum_{e \in A(u) \cap A(v)} [c_e(\Phi') - c_e(\tilde{\Phi}') - c_e(\Phi) + c_e(\tilde{\Phi})]. \quad (27)$$

Each assignment edge pair corresponds to a particular configuration, thus if a node saturates the maximum of 4 edges, 16 configurations must be queried. Additionally, since there exist edges in $A(u)$ which may not have been affected by moving node v , we need only consider contributions from edges which are adjacent to both u and v . Thus, for each edge e in $A(v)$, we update each node comprising e using only the contributions from e . If, for any node u , there is more than one common edge between u and v i.e., $|A(u) \cap A(v)| > 1$, then each contribution will be added separately to the delta gain. This must be repeated for each neighbouring node of the moved node v , for each destination. However, many values can be stored and reused. For example $c_e(\Phi)$ and $c_e(\Phi')$ will be the same in each calculation when e is the same, so we need only check the contributions from $c_e(\tilde{\Phi})$ and $c_e(\tilde{\Phi}')$. In order to perform each gain update in $\mathcal{O}(1)$ time, we must store the configuration of each edge and the contribution of each configuration to the cost. In addition, we need to store two auxiliary objects for each edge, which we will call the *root counts* and the *receiver counts*. Each of these is simply a vector of length $|P|$, where each element corresponds to the number of nodes from the root/receiver set

in a particular partition. Each move will increment either the root or the receiver counts by removing one from the source element and adding one to the destination element. The full configuration can be updated directly from the root and receiver counts, checking whether each of the counts has changed from zero to non-zero, or vice-versa. The cost can then be read from the pre-computed cost table. The pseudocode for the delta gain calculation is given in Alg. 7, while the general auxiliary functions required for the FM algorithm are given in Alg. 6. Storage and retrieval of the respective counts and configurations of each edge adds an overhead, and for small graphs it may be quicker to directly compute the edge costs to find the delta gain. However, it is necessary for maintaining the time-complexity of the full algorithm, thus the benefits are clear for larger circuit sizes. The full algorithm is given in Alg. 2.

4 Multilevel quantum circuit partitioning

The multilevel paradigm is a crucial part of the success of state-of-the-art methods for large-scale graph partitioning, as demonstrated by partitioners such as METIS [37] and KaHyPar [40]. While heuristic refinement methods, such as FM, have proved effective for small to medium problem sizes, the solution quality typically drops as problem sizes increase. This is expected as the solution space expands exponentially, making heuristics increasingly less effective at exploring the solution space. Multilevel methods employ *coarsening* routines for transforming large-scale, complex problems into smaller problems, for which good results can be obtained. This is typically followed by iterative *uncoarsening* and *refinement* of the results into a solution for the larger problem. A graph can be coarsened by merging nodes together and contracting the edges between them. There are many possible ways that a graph can be coarsened, and the choice of coarsening strategy, as well as the number of levels, can have a significant impact on the performance of the algorithm.

Quantum circuit graphs have a structure which is particularly suited to multilevel partitioning. Since each qubit is expanded into d nodes, each associated to a particular time-step, we propose

a temporal coarsening. Beginning with the fine-grained temporal hypergraph, as described in Sec. 2.3, we proceed by merging nodes along the time axis, contracting the state-edges between them, to obtain a sequence of coarser graphs. By coarsening the time axis down to a single time-step, we end up with a static hypergraph, which can be partitioned using standard methods, since there is no temporal component. Such a problem can be scaled to thousands of qubits, though the resulting solutions are unable to benefit from state teleportations, which requires state-edges to be cut. The graph is then uncoarsened by a single-level, using the solution from the previous level as a starting solution. In the coarsening phase, we store a contraction history, which tells us which nodes have been merged between each level, allowing us to transform the solution from the previous level into the new solution. The partitioning algorithm is then run again for a predefined number of passes to refine the previous result. This is repeated until the original graph is recovered and the full problem solution refined. In this way, we gradually introduce the possibility of state teleportation into the problem. While we restrict to temporal coarsening, there are still many different possible coarsening strategies, since we may merge multiple time-steps or even multiple regions of time at once. We explore three different basic coarsening strategies, which we refer to as *window*, *block* and *recursive* coarsening.

4.1 Window coarsening

The most basic uncoarsening procedure can be implemented by contracting time-intervals from d down to 0. Calling the size of each interval w , we can coarsen the graph by successively merging nodes in each interval into a single node, such that the number of time-steps is reduced by w at each level, down to 0, where the final interval may be smaller than w . After each interval has been contracted, a copy of the graph is stored for the refinement. This is referred to as *window* coarsening, since a new fine-grained time-interval is revealed at each level, like a window moving along the time axis. The pseudocode for window-based coarsening is given in Alg. 8. If we set the interval size to $w = 1$, then we reveal the graph one time-step at a time, as in Alg. 4. If instead we prefer to choose the number of levels,

we can calculate the required interval sizes as $w = d/n_{levels}$, and adjust for any remainder. The full window coarsening algorithm is given in Alg. 8 and illustrated in Fig. 7.

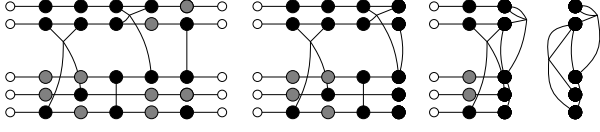


Figure 7: Illustration of the window-based coarsening procedure.

Algorithm 3: Single-Layer Time Contraction for a Temporal Hypergraph (**ContractTime**)

Input: $H = (V, E)$: A hypergraph whose nodes are (q, t) indicating qubit q at time t .

src: The source time-layer to be merged.

trg: The target time-layer into which the nodes at src will be merged.

Output: A new hypergraph H' in which all nodes at time-layer src have been merged into trg.

ContractTime(H , src, trg) $H' \leftarrow H$;
 $V^{(src)} \leftarrow \{v \in V \mid v = (q, t), t = \text{src}\}$;

foreach $v \in V^{(src)}$ **do**

- $u \leftarrow (q, \text{trg});$
- remove self-loop (v, u) from E_s ;
// Remove any self-loops.
- foreach** $e \in E$ **such that** $v \in e$ **do**
 - if** $v \in e_{\text{root}}$ **then**
 - $e_{\text{root}} \leftarrow e_{\text{root}} \setminus \{v\};$
 - $e_{\text{root}} \leftarrow e_{\text{root}} \cup \{u\};$
 - else if** $v \in e_{\text{rec}}$ **then**
 - $e_{\text{rec}} \leftarrow e_{\text{rec}} \setminus \{v\};$
 - $e_{\text{rec}} \leftarrow e_{\text{rec}} \cup \{u\};$

$V \leftarrow V \setminus V^{(src)};$ *// Remove original src-layer nodes*
return H' ;

4.2 Block coarsening

We may also coarsen the graph into blocks of nodes by contracting one time-step in each block per level. In this case, the size of each block b corresponds to the number of levels, since we uncoarsen one time-step per block at each level. We

Algorithm 4: Full Coarsening of a Temporal Hypergraph (**CoarsenGraphFull**)

Input: $H_0 = (V_0, E_0)$: original (fine) hypergraph with time-layers $[0, \dots, \text{depth}]$;

depth: maximum time-layer index

Output: Sequence $[H_0, \dots, H_{\text{depth}-2}]$ of hypergraphs

CoarsenGraphFull(H_0 , depth) $hList \leftarrow [H_0];$ *// Store coarsening hierarchy*
 $H \leftarrow H_0;$ *// Working copy*

for $\ell \leftarrow \text{depth}$ **to** 1 **do**

$H' \leftarrow \text{ContractTime}(H, \ell, \ell - 1);$

$hList.append(H');$

$H \leftarrow H';$

return $hList;$

may also choose to coarsen all blocks down to a single time-step. We can either set the number of blocks and calculate the block size from $b = d/n_{blocks}$, or choose the blocks size directly. The pseudocode is given in Alg. 8.

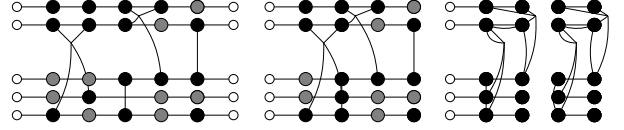


Figure 8: Illustration of the block-based coarsening procedure.

4.3 Recursive coarsening

The final method considered is referred to as *recursive* coarsening. We divide the graph into adjacent pairs of time-steps then merge the nodes between them at each level. The number of nodes thus decreases exponentially with each level, making the number of levels is automatically $\log_2(d)$, unless we choose to cap it earlier. Pseudocode for recursive coarsening is given in Alg. 10.

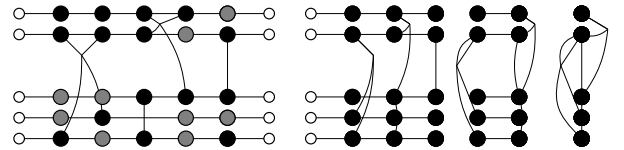


Figure 9: Illustration of the recursive coarsening procedure.

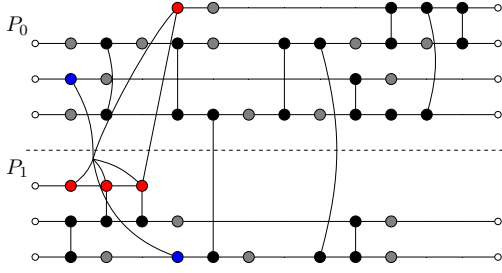


Figure 10: Partitioned graph with nested state teleportation. The highlighted hyper-edge has four root nodes (red) and two receiver nodes (blue). Both the receiver nodes and the root nodes span across P_0 and P_1 , indicating the presence of a nested state teleportation. According to Eq. 17, the hyper-edge cost is 0. A starting process is performed from P_0 to P_1 , but since the root node ends in P_1 , the ending process is used to teleport the state to P_1 . The ‘cost’ is accounted for by the cut state-edge. Partial circuit shown in Fig. 11 and full circuit in Fig. 13.

5 Circuit extraction

The final step in the workflow is to extract the circuit from the partitioned graph and the assignment function. Since the partitioned circuit will require entanglement distribution, we need to have some number of ancillary communication qubits in each QPU. If we have not used a gate grouping pass then communication qubit requirements are modest, since they are released immediately after each state and gate teleportation. However, if we have used gate grouping, there is likely to be a requirement for multiple communication qubits to be active at the same time, demanding larger communication qubit capacities. We choose to start with a predefined number of communication qubits, though allow the possibility to dynamically add communication qubits as needed. While this may not be something that is supported by physical architectures, spare data qubits may also be considered as pseudo communication qubits for links which are kept active over many time-steps. Pseudo communication qubits may not be able to generate e-bits, but can store states linked from starting processes to free up additional communication qubits. If this is not possible, then we may have to collapse and the link with an early ending process. The previous teleportation procedure may then be restarted, at the cost of an additional e-bit. Naturally, this method will increase the depth of the resulting circuit and may introduce additional noise. We

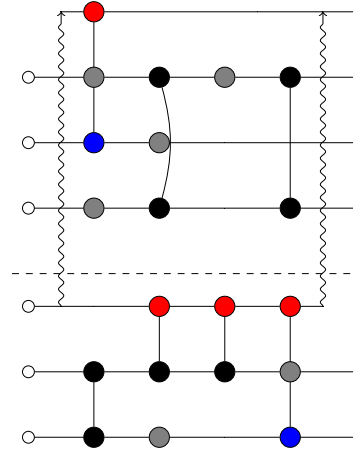


Figure 11: Partially constructed circuit to cover the hyper-edge in Fig. 10, starting process is used to cover the first receiver gate, which is then converted into a nested state teleportation by redirecting the ending process. Full extracted circuit is shown in Fig. 13.

explore this trade-off further in Sec. 7.2. Assuming we have sufficient communication qubit capacity, we proceed as follows.

We start by creating a d -dimensional, empty list L , representing the time-steps of the original circuit. We then pass through the gate edges and hyper-edges in the graph in order of time, appending operations to the corresponding entry in the list. For each cut state-edge, we schedule a state teleportation. For each gate edge, including hyper-edges, we check the receiver assignment set. For each local receiver we schedule a local two-qubit gate. For each non-local receiver, we schedule a starting to the receiver partition. We record the partitions associated with all root nodes, and store these to schedule the ending process later. We then insert each two-qubit gate into the appropriate time-step of the circuit, replacing the root qubit argument with the corresponding communication qubit. If we encounter a cut-state edge while the root qubit is still active, we delay the teleportation until all gates in the group have been completed, after which we insert ending processes directed towards the final partition of the root. If we encounter an anti-diagonal single-qubit gate which occurs on the root qubit of an active group, we apply an X gate to each linked communication qubit, as well as the root, as described in Sec. 2.2.1. This routine is sufficient to cover all of the non-local gates with the required e-bits. In future work, we aim to identify further avenues for optimisation, such as gate

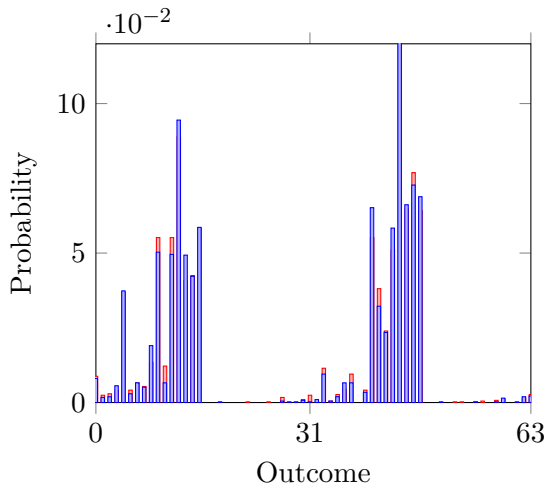


Figure 12: Comparison of the output distribution of the original circuit with that of the partitioned circuit, generated using the Qiskit Sampler. The partitioned graph is shown in Fig. 10 and the output circuit in Fig. 13. The output distribution of the partitioned circuit matches the original.

commutation within groups. The above procedure is sufficient for extracting a circuit with at the desired e-bit cost, though may still require further compilation within each sub-circuit. An implementation of the circuit extraction is available in the `disqco` repository [58].

In order to ensure that the circuit is correctly extracted, we must ensure that the extracted circuit is equivalent to the original circuit. We can do this by simulating the resulting circuits and comparing the output distribution with that of the original circuit. The extracted circuit is a Qiskit circuit object, and which can be simulated within the Qiskit framework, or converted to a QASM file for simulation on other simulators. We use the Qiskit sampler primitive to perform the simulation. In Figure 12 we compare the output distribution of a random 8-qubit circuit with the output distribution of the circuit extracted from the partitioned graph. This also allows us to compare the depth of the original circuit with the extracted circuit, as well as the demand for communication qubits. Typically, if gate grouping is used, the resulting depth is reduced, since the entanglement requirements are lower, while the demand for communication qubits is higher. The extracted circuit is then ready for further optimisation, such as gate synthesis, or for direct implementation on a quantum computer.

6 Implementation details

6.1 Complexity of FM for quantum circuits

The time complexity of the original FM algorithm, for bi-partitioning, is linear in the number of nodes, provided that the gain updates can be performed in constant time. Each pass requires the gain of each node to be queried once when initialising the buckets, for time $\mathcal{O}(n)$, after which each node is moved once, updating the gains of all neighbours. This means the gains of the neighbours must be updated n times per pass. If there is no bound on the number of neighbours, this results in a time complexity $\mathcal{O}(n^2)$, since each node has a maximum of $n - 1$ neighbours. However, in many realistic scenarios, the maximum number of neighbours is bounded by a constant which is much smaller than the total number of nodes in the graph. If we have such a bound on the number of neighbours, and each delta gain calculation is $\mathcal{O}(1)$ for each of these neighbours, we have a time complexity $\mathcal{O}(n)$ for both the initialisation and the main loop, giving $\mathcal{O}(n)$ overall. When extending to multi-partitioning, the complexity increases linearly with the number of partitions, since the cost of moving each node must be calculated for each external partition. This makes the pass complexity $\mathcal{O}(kn)$, where k is the number of partitions.

While the algorithm structure is similar for quantum circuit graphs, the number of nodes is in fact equal to the number of qubits n_q times the depth of the circuit d , such that bi-partitioning has complexity $\mathcal{O}(n_q d)$, making the pass complexity for k -partitioning $\mathcal{O}(kn_q d)$. Sec. 2.3 shows how to perform the gain updates in constant time for the temporal hypergraph, provided the costs of all hyper-edge configurations are pre-computed. We note that the complexity of the pre-computation is exponential in the number of partitions, since there are exponentially many possible edge configurations which must be pre-computed. However, since k is typically much smaller than n_q , this has a negligible effect up to 20 partitions. Scaling beyond this, however, becomes challenging. We discuss some potential strategies for this in App. A.4. Without gate grouping, the number of neighbours is bounded by 3, so the time complexity is maintained. However, after gate grouping, the upper bound of the number of neighbours scales with d , since this is

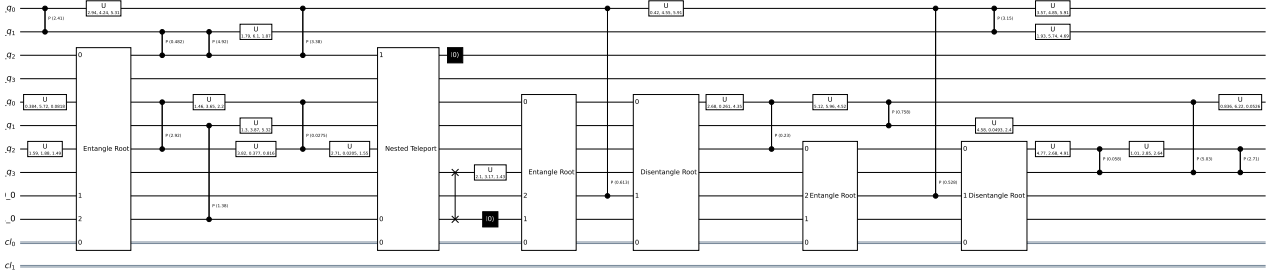


Figure 13: Circuit extracted from the partitioned graph in Fig. 10. Each instruction related to communication occurs in a custom box spanning the data qubits, communication qubits and classical bits involved. The first custom box is an entanglement starting process, while the second custom box completes the nested state teleportation by collapsing the state onto the linked communication qubit. This qubit is then swapped to a data qubit slot at the destination. The second box requires no additional e-bits, since the gate teleportation has been started already. Three e-bits are used, in total.

the maximum number of gates which could exist in a group. For most circuit types, the groups will be far from this threshold. However, there do exist some circuit structures which lead to very large groups. Such circuits are more computationally intensive to optimise, though typically result in a low proportion of e-bits to gates. The pass complexity, in this worst case, is $\mathcal{O}(kn_q d^2)$. If a constant number of passes is used, the total complexity is $\mathcal{O}(kn_q d^2)$.

6.2 Improving efficiency of FM

When dealing with large circuits, it may be necessary to look for adaptations to increase the efficiency. Firstly, it should be noted that moving every node once is an unnecessary requirement to enforce for large graphs, since typically the iteration of best gain is achieved relatively early (quantify) in the pass. We can, therefore, limit the number of nodes which are moved in a pass. The limitation of this is that we become less likely to escape a local minimum. There are a number of possibilities for remedying this – we choose to alternate between exploratory and exploitative passes. Exploitative passes are the normal passes defined in Alg. 2. Exploratory passes, on the other hand, still seek to make the best move at each iteration, but *do not* roll-back to the iteration of best gain at the end of the pass. As a result, the cost will often increase after an exploratory pass, but will tend to decrease on average. We find this to be effective provided we are limiting the number of moves to

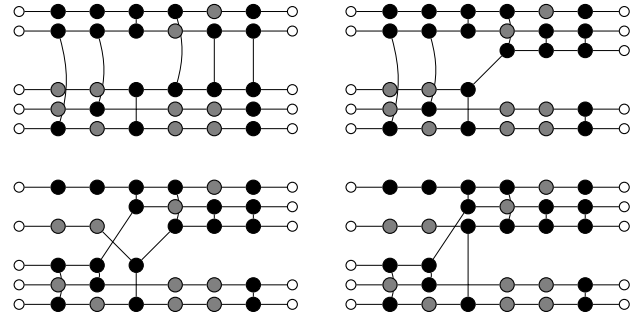


Figure 14: Illustration of a local minimum in the circuit optimization process.

a small ($\approx 0.1n_q d$) subset of nodes. We compare the effect of using exploration vs only exploiting in Fig. 20a. Clearly, while cost changes much more rapidly in the case of exploratory method, the minimum value is often significantly lower, despite the fact that the exploratory method is performing fewer moves overall.

6.3 Avoiding local minima

FM is a local search heuristic, meaning that it locally modifies problem solutions in search of improvement. Often such methods are susceptible to becoming stuck in local minima after quickly reaching arrangements which cannot be improved with a single action. FM is designed to avoid this by enforcing the movement of all nodes in a single pass, whether or not any improvement is made. This allows the algorithm to explore

a large region of the space of solutions. This is particularly important in the case of temporally extended graphs, where it may often take a series of local moves to find a benefit. However, dealing with individual nodes permits fine-grained control over the larger possible actions which can be built, allowing nodes to be moved in particular regions of the circuit which may be beneficial. This allows us to achieve complex, but efficient, final distributions of quantum circuits. We illustrate this point using the example in Figure 14. The initial partition is *static* in the sense that $\Phi(v_i^{(0)}) = \Phi(v_i^{(t)})$ for all $t = 0, 1, \dots, d - 1$. This is a local minimum, since each node has two local state edges (except for nodes $v_i^{(0)}$ and $v_i^{(d)}$, which have one state edge but no gate edges) and a maximum of one gate edge, since no nodes have been merged. As a result, the best local action can only increase the total cost by 1. However, after one of these actions has been taken, this creates an avenue to explore larger actions, since the update will decrease the cost of moving neighbouring nodes. In Figure 14, we see that the next best action is to move the node $v_i^{(1)}$ for a cost increase of 0, followed by $v_i^{(2)}$, until eventually a cost decrease is obtained by creating a local gate edge. This path of moves will be explored as far as gives benefit, until node $v_i^{(d)}$ is reached or a better action becomes available. This same is true after the graph has undergone gate grouping. Since a node can simultaneously be a receiver node and a root node in a group, the maximum amount of edges a node can be involved in increases to 4. Each gate group contributes a maximum of k to the cost, where k is the number of partitions connected. Moving a single node to another partition can only change the cost by a maximum of ± 4 , with 2 possible contributions from state edges and two from gate edges. When all state edges are local, as in the initial static assignment, no single move can decrease the cost. The example in Figure 14 illustrates a series of local minimum escapes via a number of move sequences. Note that, once graphs have been coarsened, this is no longer true, since the bound on the number of edges per node increases with the number of contractions. However, when we move coarsened nodes, we are effectively moving multiple time-adjacent nodes at once, which has the same effect as sequences of moves. In this way, exploration is less important at coarser levels, but becomes

increasingly necessary for finer levels.

6.4 Complexity of multilevel FM

While we still perform the partitioning algorithm at each level of the multilevel framework, we gain a speed up from the fact that, at coarser levels, the number of nodes is reduced. In general, each pass has a complexity $\mathcal{O}(k|V| \max_{v \in V} |N(v)|)$, where $|V|$ is the number of nodes in the graph, and $\max_{v \in V} |N_H(v)|$ is the maximum number of neighbours a node may have. When we coarsen, we decrease both the number of nodes in the graph and max number of neighbours of each node. However, the total complexity is not reduced if we still uncoarsen to the finest level, since this level will dominate the scaling. This is demonstrated in Fig. 22b, where the slope of each of the multilevel methods starts flat, and steepens with each level until it reaches the finest, where the slope matches the standard FM approach. However, there are approaches we can take to reduce the complexity of the finer levels. The complexity of multilevel methods are determined by the pass complexity of the finest phase of partitioning and the number of levels. If the finest graph used is the original graph, and the number of levels is predefined, then there is no change to the complexity. However, when dealing with large circuits, we may restrict the finest phase used to reduce the required computation. For example, if we temporally coarsen the graph down to n_q nodes, we reduce the number of nodes as well as the maximum number of neighbours, which goes from $\mathcal{O}(d)$ to $\mathcal{O}(n_q)$. However, each will now be involved in more edges, for a maximum of d , if it has a gate-edge at each time-step. However, if it has an independent gate edge from each time-step, then each of these must connect to a single other neighbour, meaning we need only update one neighbour per edge. Alternatively, if the node is involved in hyper-edges, the same restriction applies, since each time-step over which the hyper-edge spans constitutes a time-step in which the node can't be involved in another hyper-edge or gate-edge. Thus, even though we have coarsened the maximum number of neighbours to n_q , the maximum number of contributions to the delta gain is still d . So the pass complexity at the coarsest level is $\mathcal{O}(kn_qd)$. As we uncoarsen, we regain the additional factor of d in the complexity due to the increased

number of nodes. However, due to the increased effectiveness of the coarser levels, we can put a firmer cap on the number of nodes moved at each pass. If we limit the number of nodes moved to n_q , then we retain the pass complexity $\mathcal{O}(kn_qd)$, with an additional factor for the number of levels we use. In practice, the length of passes will still change between levels due to specific differences based on the coarsening strategy used, but these do not affect the scaling of the algorithm. For fairness of comparison, we use the same number of levels for each coarsening strategy. In the recursive coarsening strategy, since we coarsen pairs of nodes at each level, the resulting number of levels is logarithmic in the depth of the circuit. Thus, in all tests, we use $\log_2(d)$ coarsening levels. The resulting complexity of each of the multilevel methods is $\mathcal{O}(kn_qd \log_2(d))$. In Sec. 7.4, we experimentally compare the speed and performance of each method.

7 Results

A number of different tests are run to benchmark the performance of the different workflows. Recalling the sequence of stages in the framework, we have *transpilation*, *gate grouping*, *graph conversion*, *coarsening*, *partitioning*, *uncoarsening/refinement* and *circuit extraction*. Not all of these phases are varied in the benchmarking, notably, transpilation, graph conversion and circuit extraction remain the same in all cases. We use the basic Qiskit transpiler into the gate set described in Eq. 14 and custom built functions for building the graphs and extracting circuits. For gate grouping, we investigate only the *greedy gate grouping* method, described by Alg. 1, and the trivial case of no gate grouping. For coarsening, we investigate the basic FM with no coarsening, the window-based multilevel method, MLFM-W, the block-based method, MLFM-B, and the recursive method, MLFM-R. For the partitioning algorithm, we briefly compare the FM algorithm with the exploratory variant. In all cases it is assumed that each QPU has the same number of qubits, all containing one additional space to facilitate state teleportation. We make no assumptions on the number of communication qubits.

All tests are performed on a MacBook Pro M3 Pro with 18GB RAM and an 11-core CPU containing 6 performance cores and 5 efficiency cores,

with performances cores clocked at 4.05 GHz and efficiency cores at 2.8 GHz. All code used to generate the results is available in the `disqco` repository [58].

7.1 Benchmark circuits

The set of circuits to be used in benchmarking is chosen such as to cover a wide-spectrum of circuit structures. This allows us to identify cases where existing methods perform well, and cases where they do not, while demonstrating the consistency of the proposed framework in all cases. This also allows us to draw some conclusions about which circuits are best suited to which methods of non-local gate coverage.

7.1.1 CP-fraction

CP-fraction circuits are a generalisation of the *CZ-fraction* circuits introduced by Sundaram et al. [59]. These circuits provide a useful tool for benchmarking the performance of circuit partitioning and distribution algorithms, since the proportion of two-qubit gates can be varied for a fixed depth and number of qubits. The CP-fraction variant was introduced in Ref. [53], as a means of generalising to a universal gate set, since transpiled CZ-fraction circuits often lose depth due to commutation relations between Hadamard gates and CZ gates. A CP-fraction circuit can be constructed as follows. For a given probability p , qubit count n_q and depth d , single-qubit gates are applied to each qubit with probability $1 - p$, while the remaining qubits are paired and acted on with two-qubit gates. This is repeated up to depth d . We use $U(\theta, \phi, \lambda)$ and $CP(\theta)$ gates with randomised parameters.

7.1.2 Quantum Fourier transform

The quantum Fourier transform (QFT) is a well-known quantum sub-routine which is used as a subroutine in various quantum algorithms. The prevalence of the QFT make it an essential benchmark circuit. The circuit can be built entirely using controlled-phase ($CP(\theta)$) gates and Hadamard H gates. Long chains of contiguous $CP(\theta)$ gates lead to very large hyper-edges, so the entanglement cost of a distributed QFT is typically low for methods permitting gate grouping. Furthermore, it is observed that in our framework, the lowest entanglement cost is achieved

using the trivial, initial placement of qubits, indicating that the initial placement is a global optimal for this structure. We note that similar results have been found elsewhere [60].

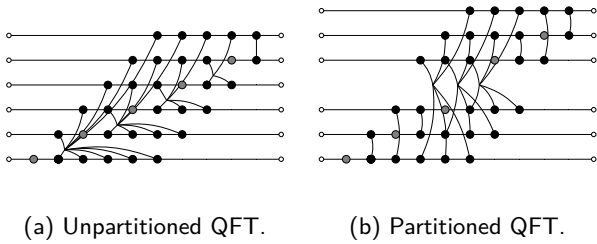


Figure 15: 6-qubit QFT graph after gate grouping. After partitioning, we remove all local contributions to hyper-edges. Note that, with gate grouping, the optimised result is the same as the initial placement.

7.1.3 Quantum volume

Quantum volume (QV) circuits, introduced by Cross et al. [61], are designed to benchmark the performance of quantum computers. QV circuits consist of layers of Haar random unitaries selected from $SU(4)$, applied to randomly chosen pairs of qubits. QV circuits provide a nice balance between structure and randomness, since the decomposed layers require the same qubits to interact for a number of time-steps before the next layer is applied. Notably, since the unitaries are chosen randomly, decomposed two qubit-gates are unlikely to contain potential for gate grouping, since the resulting blocks do not contain contiguous $CP(\theta)$ gates, and any single-qubit gates are unlikely to be diagonal (or anti-diagonal). As a result, methods that are reliant on gate teleportation typically perform poorly, while methods employing state teleportation perform well, as observed in Ref. [53]. For all tests, we set the number of layers to be equal to the number of qubits.

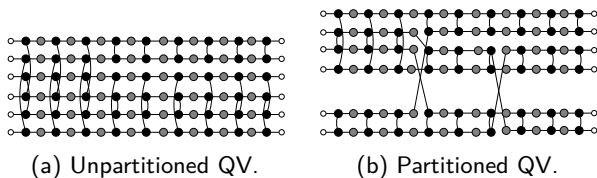


Figure 16: Example graph from 6-qubit from QV circuit. Note that the grouping algorithm has no effect on QV circuits, since there are no contiguous $CP(\theta)$ gates and random unitaries are unlikely to decompose into diagonal or anti-diagonal single-qubit gates.

7.1.4 Quantum approximate optimisation algorithm

The quantum approximate optimisation algorithm (QAOA) was introduced as a method for efficiently solving hard combinatorial optimisation problems, such as MaxCut and MaxSat [62]. QAOA circuits comprise parameterised single- and two-qubit gates, for which the parameters are classically optimised to find an approximately optimal solution. We consider randomly initialised QAOA circuits for MaxCut problems over random graphs with an edge probability of 50%. QAOA circuits, like QFT, permit large groups of gates for multi-gate teleportation.

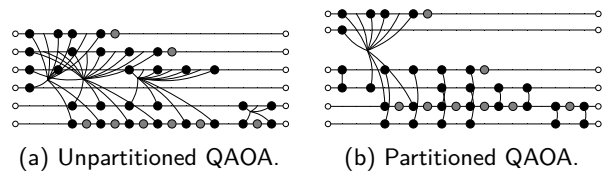


Figure 17: Example graph from 6-qubit QAOA circuit. Circuit is a randomly initialised instance of QAOA for MaxCut over a random graph with edge probability 50%.

7.1.5 QASM benchmark suite

In addition to the circuits described above, we test on a number of circuits provided by the QASM benchmark suite [63]. We test on all circuits in the large below depth 1000 after transpilation, excluding QFT and QV since they are tested separately.

7.2 Benefits and limitations of gate grouping

7.2.1 Reduced entanglement requirements

Here we provide a brief demonstration of the benefits and limitations of gate grouping. Using the CP fraction benchmark circuits, we vary the fraction of two-qubit gates, for a constant depth and qubit count of 32, partitioning the resulting circuits across 4 QPUs. In Fig. 18, we plot the distributions of the entanglement costs achieved for 100 randomly generated CP fraction circuits. While the effects are less noticeable for low fractions, the benefits of gate grouping become apparent as the fraction of two-qubit gates increases, where the distribution of the results with gate grouping is shifted towards lower cost. However, this can come at an extra cost in time as the fraction approaches 1, since the gain updates must

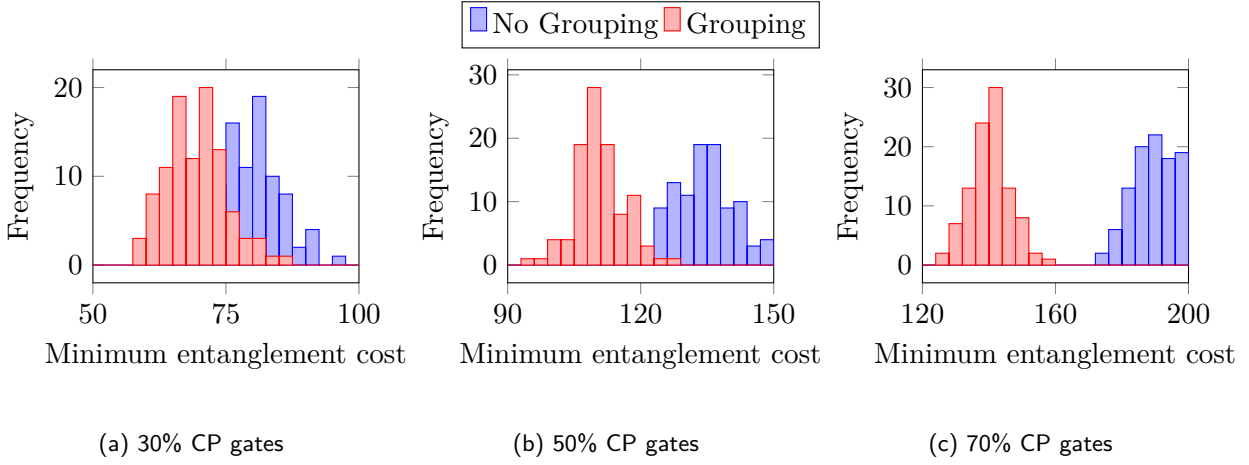


Figure 18: E-bit reduction from gate grouping. As the fraction of two-qubit gates increases, gates are grouped into larger hyper-edges, allowing for reduced entanglement costs via multi-gate teleportation. Plots produced from 100 runs of FM, on a 32-qubit CP-fraction circuit with depth 32, partitioned across 4 QPUs.

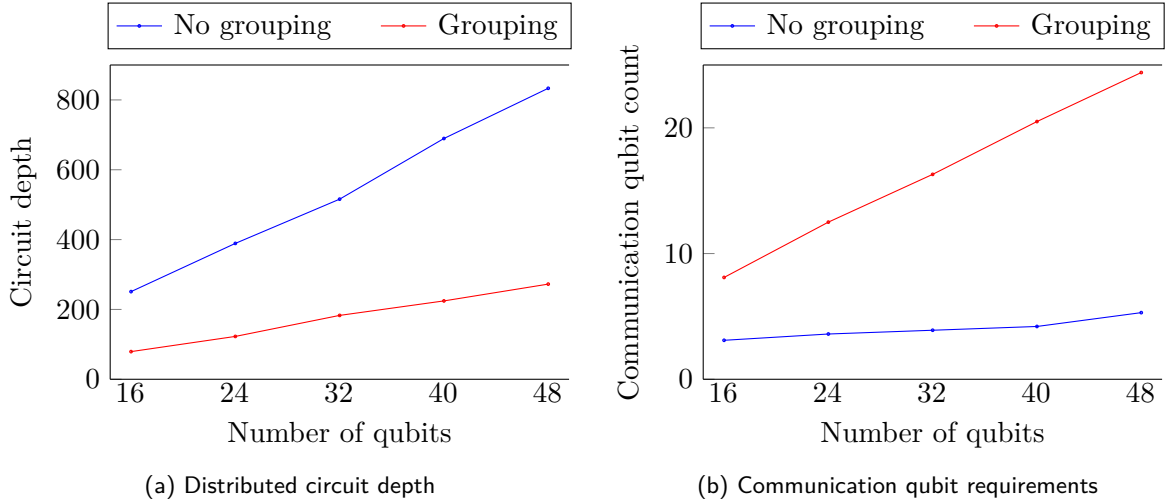


Figure 19: Comparison of circuit depth and communication qubit requirements with and without gate grouping. The means results are shown from 10 runs of FM on QFT circuits, each partitioned over 4 QPUs. The circuit depth is significantly reduced when using gate grouping, though this is compensated by an increase in the number of communication qubits required.

be performed over very large hyper-edges. Additionally, as discussed in Sec. 5, the demand for communication qubits increases as the fraction of two-qubit gates increases. Without multi-gate teleportation, communication qubits are released immediately after use, while multi-gate teleportation requires communication qubits to be kept alive for the duration of the group. Conversely, a large communication qubit capacity reduces the additional communication depth, since entanglement can be generated in parallel.

7.2.2 Increased communication qubit requirements

A notable limitation of the current work is that there are no constraints placed on the number of communication qubits permitted. This is of significance when considering instances of hypergraph with large hyper-edges, since a large cut hyper-edge corresponds to a communication qubit being used over a large number of time steps. Facilitating multiple linked root qubits concurrently may require a large number of communication qubits. The benefit of not using cat-entanglements is that we only require a fewer communication qubits, since each gate teleporta-

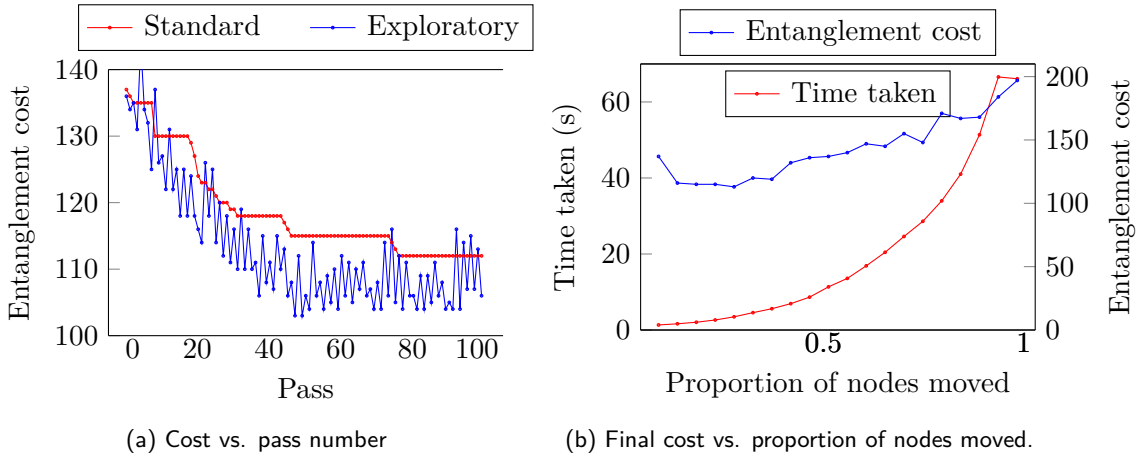


Figure 20: Illustration of the exploratory process to avoid local minima in FM. Fig. 20a shows the entanglement cost of the circuit after each pass. The cost in the exploratory method fluctuates significantly between passes but ultimately reaches lower cost as it is able to escape local minima. Fig. 20b indicates that the exploratory method is more effective when the number of moves per pass is limited. The optimal region is between 0.1 and 0.2 of the total number of nodes. Consequently, the exploratory method achieves lower costs and is faster than the standard FM algorithm.

tion and each state teleportation results in communication qubits being released immediately after use, unlike for multi-gate teleportation. The only time way may require additional communication qubits is if we need to handle multiple state teleportations at the same time-step, though still any additional communication qubits are freed up directly after use. The trade-off that we will likely end up with a deeper circuit, requiring more entanglement distribution. We briefly numerically analyse this trade-off with the following experiment on QFT circuits. For each circuit, we run the standard FM algorithm, with and without using the gate-grouping pass. When extracting the circuit, we plot both the resulting depth and the communication qubit requirements. It can be seen that the number of communication qubits required is constant when not using gate grouping, while the circuits are significantly deeper. On the other hand, the gate-grouping pass gives us a much shallower circuit, but has an increasing communication qubit requirement. The choice of whether not to use gate grouping should be made on the basis of additional qubit capacity. Additionally, we hope the lower e-bit costs from gate grouping serves to guide future DQC architectures to not under-allocate communication qubits, since they permit significantly reduced circuit depth.

7.3 Exploratory vs exploitative FM

Here we demonstrate a tweak made to the typical FM algorithm structure which proved particularly effective for avoiding local optima. The method involves alternating between exploratory and exploitative passes, where the former does not roll-back to the iteration of best gain at the end of the pass. This allows the algorithm to explore larger sequences of moves which may allow the same node to be moved multiple times before a roll-back. We find that this is most effective when the number of nodes moved in each pass is limited, since the algorithm is less likely to escape a local minimum. This has an added benefit of providing a reduction of the pass time. However, we typically use a constant fraction of the number of nodes, so this reduction is only constant. The results are shown in Figure 20.

7.4 Multilevel partitioning

We compare the cost and time performance of the coarsening routines described in Sec. 4. Partitioning is performed using no coarsening (FM), window coarsening (MLFM-W) 4.1, block coarsening (MLFM-B) 4.2 and recursive coarsening (MLFM-R) 4.3. In Fig. 21, we show the entanglement cost and time taken as function of the number of passes for each method. For each of the multilevel methods, we run 10 passes at each level, and for FM we run $10\lceil\log_2(d)\rceil$ passes, such

that the total number of passes is the same in all cases. Fig. 21a shows the entanglement cost after each pass, demonstrating the improved performance of the multilevel methods. After each 10 passes, the entanglement cost plateaus, indicating that the methods are reaching a local optimum for the given level, which is then quickly improved upon at the next level. Fig. 21b shows the time taken for each pass, demonstrating that improvement in run time of coarser passes. Notably, the last 10 passes are performed at the finest level of granularity, such that there is no improvement on the pass time. However, the overall time taken is significantly reduced due to the reduced number of nodes at coarser levels. Fig. 21c and 21d employ the exploratory method with a cap on the number of nodes moved per pass. The cap is set to $0.125n_qd$ (the optimal proportion of nodes to move from Fig. 20b) for the fine-grained FM method and n_q for the multilevel methods, since the performance is retained for fewer node moves. We see similar results for the entanglement costs, while the time taken is much lower for all methods. Interestingly, for the recursive method, the time per pass is longer at coarser levels. This is potentially due to the fact that, while the nodes moved per pass is reduced, the number of edges in which each node is involved is higher at coarser levels. Overall, however, the time taken is greatly reduced.

The results in Fig. 22 are generated using the same parameters as Fig. 21c and 21d. With the move cap in place the window method is the fastest, though shows little advantage over standard FM in cost. The recursive method maintains the lowest entanglement costs and, for larger circuit sizes, is the largest.

7.5 Benchmark algorithms

In order to compare the performance of the multilevel framework, we compare the results with the best performing methods from the literature. We use a number of workflows from Pytket-DQC [64], which are the subject of References [56, 20, 65], and the fine-grained partitioning method from Ref. [23]. We use the best performing pipeline from our methods, which uses the recursive coarsening method and the exploratory FM algorithm. The number of moves per pass as capped at n_q , as discussed in Sec. 6.4, and 10 passes are performed at each level. Below we describe the methods

used for comparison.

7.5.1 Pytket-DQC

Pytket-DQC is a freely available python library within Tket, Quantinuum’s open-source quantum computing toolkit [66], which contains various methods for quantum circuit optimisation. Pytket-DQC is an extension which contains a number of tools for distributing quantum circuits over multiple QPUs. The optimisation techniques available are the subject of References [56, 20, 65]. The most basic workflow available, referred to as *Partition* (P) is a static hypergraph partitioning framework [56], which employs KaHyPar [40] to obtain low cost assignments of qubits to QPUs and leverages *detached gates* to reduce entanglement costs [55]. The methods of Ref. [20] are integrated into Pytket-DQC, which uses minimum vertex cover and embedding techniques to reduce the entanglement costs of the circuit. These methods are combined in Ref. [55], with additional workflows for refining the results. The best performing workflow, based on the results in Ref. [55], is the *CoverEmbedSteinerDetached* (ESD) method, which uses various methods to refine an initial partition, though the combination of techniques means it is also the slowest. The fastest method is Partition (P), since KaHyPar is a highly optimised library written in C++. Despite being the quickest, the performance of Partition is often comparable with the more advanced techniques. A method for refining the result of Partition to incorporate embedding is also available, referred to as PartitionEmbed (PE). This method is slower than Partition, but faster than EmbedSteinerDetached, and tends to achieve better results than Partition. None of the methods available make use of state teleportation, resulting in certain cases where all techniques underperform (30). We compare results with Partition, PartitionEmbed and EmbedSteinerDetached where applicable.

7.5.2 Fine-grained partitioning

A pioneering technique in the quantum circuit partitioning literature was introduced by Baker et al. [23]. The paper provides a method for covering all non-local gates using state teleportation, via a technique referred to as fine-grained partitioning. The essence of the method is to split a

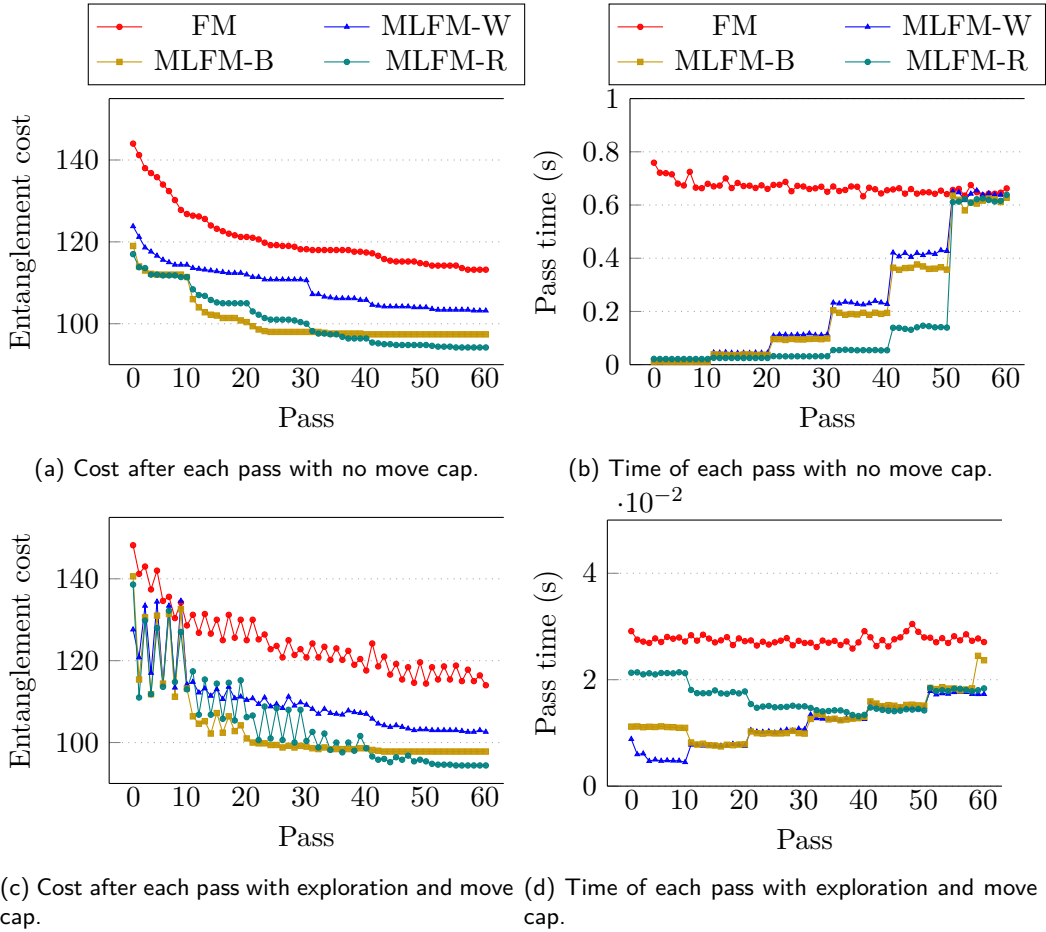


Figure 21: Performance results of the coarsening methods. All results are produced from 10 runs on a 32-qubit CP-fraction circuit with depth 32 and 50% two-qubit gates, partitioned across 4 QPUs. In Fig. 21a and 21b, we implement no limit on the number of nodes moved per pass, such that the time of the pass scales with the number of nodes in the graph. In Fig. 21c and 21d, we place a cap of n_q on the number of nodes moved per pass for the ML methods, as discussed in Sec. 6.4.

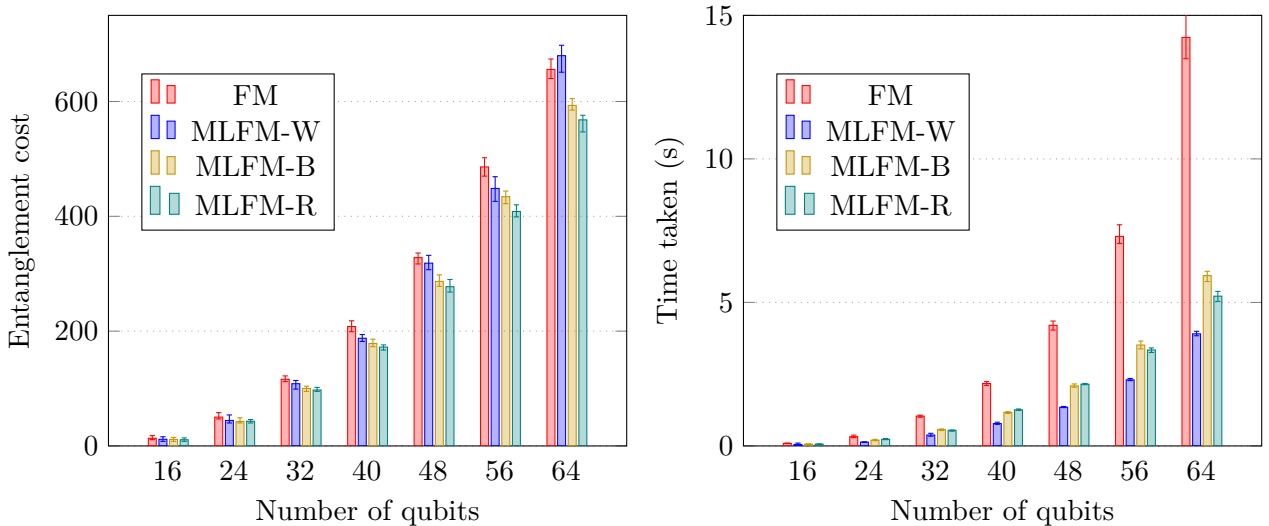


Figure 22: Performance results of the coarsening methods in terms of entanglement cost and time.

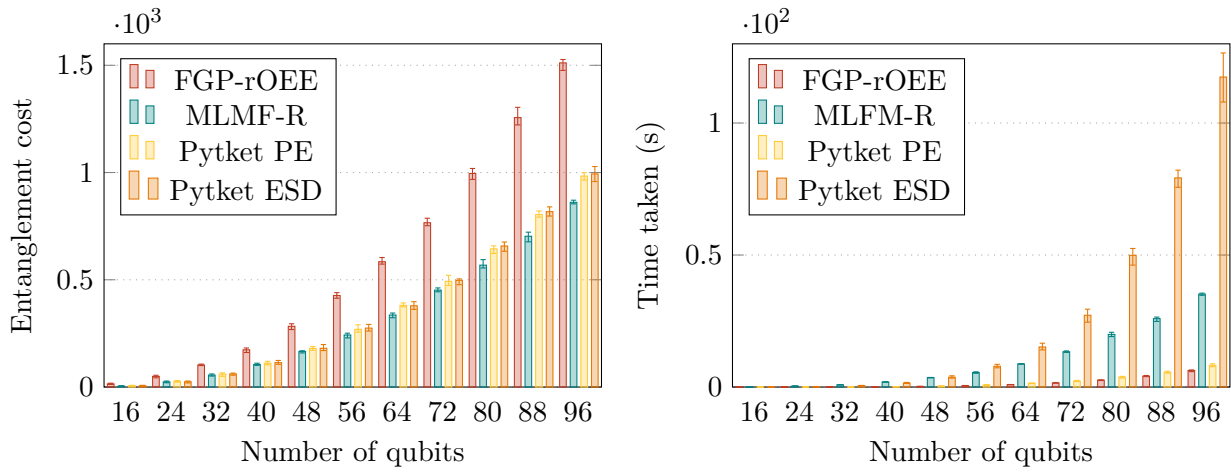


Figure 23: Circuit with 30% two-qubit gates. Starting with two QPUs for a 16 qubit circuit, for each increase in number of qubits we add a new QPU to the system. Each QPU has 9 qubit slots, which leaves a potential free data slot for teleportation on each QPU.

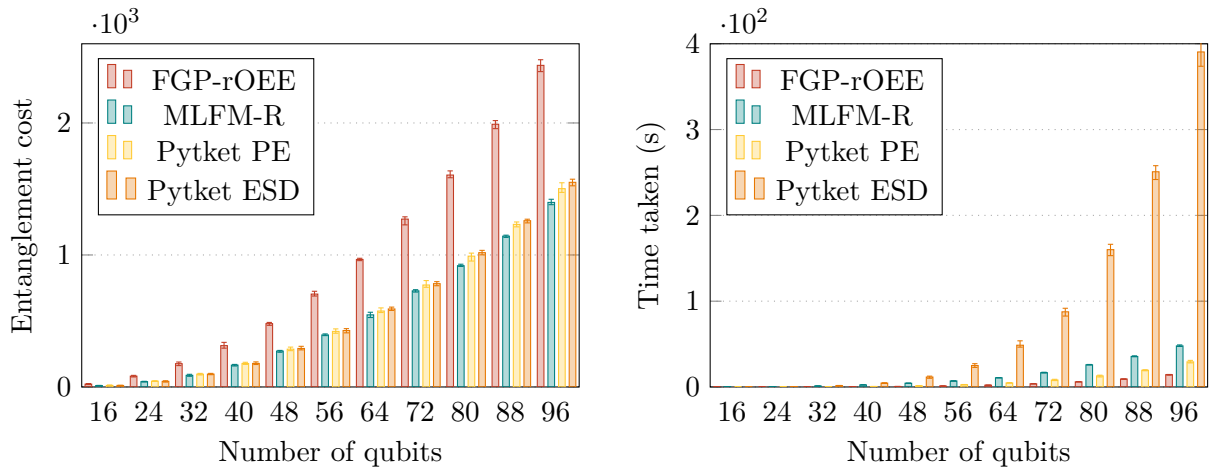


Figure 24: Circuit with 50% two-qubit gates.

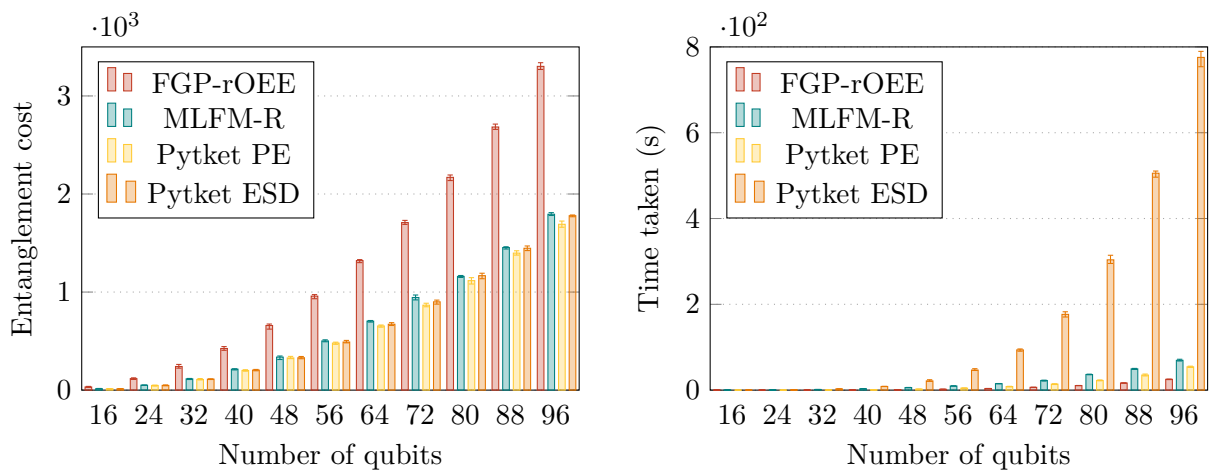


Figure 25: Circuit with 70% two-qubit gates.

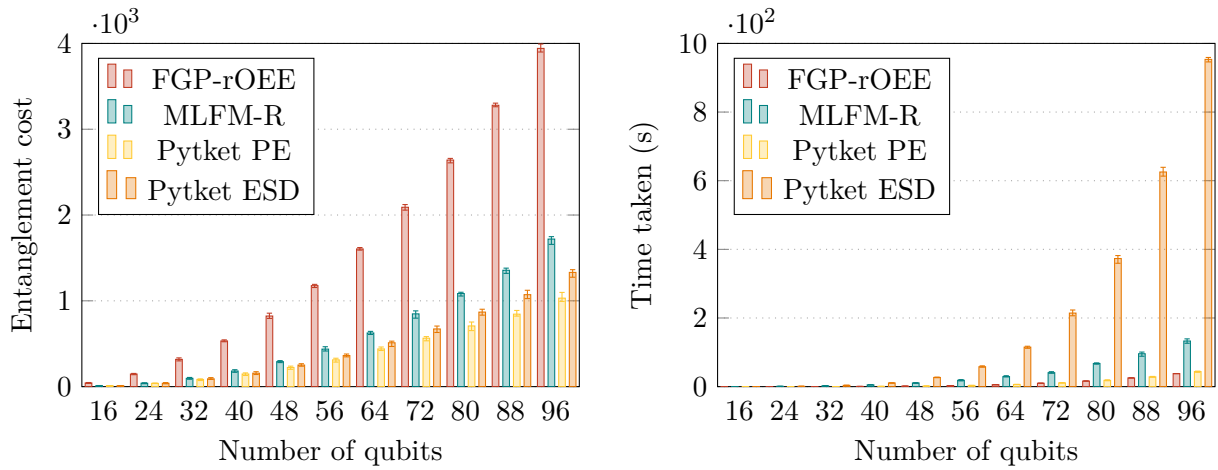


Figure 26: Circuit with 90% two-qubit gates.

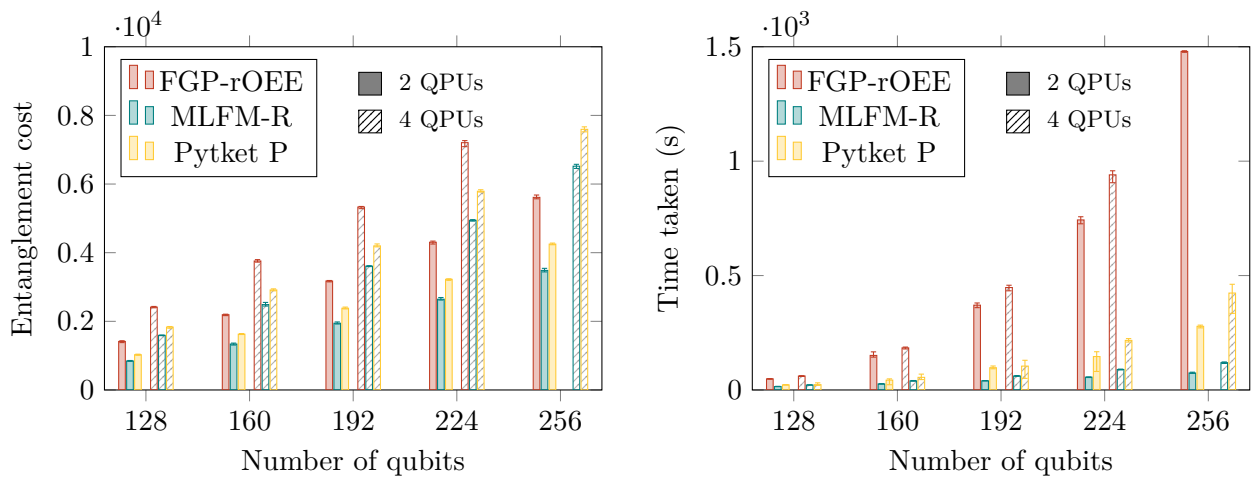


Figure 27: Large CP-fraction circuits with 50% two-qubit gates, partitioned over 2 and 4 QPUs.

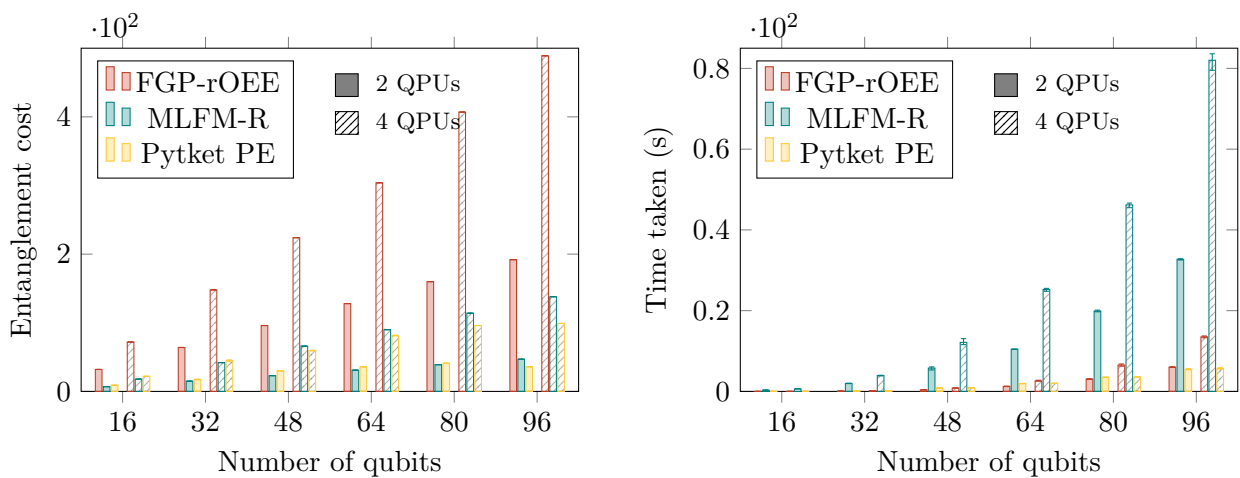


Figure 28: QFT circuits partitioned over 2 and 4 QPUs.

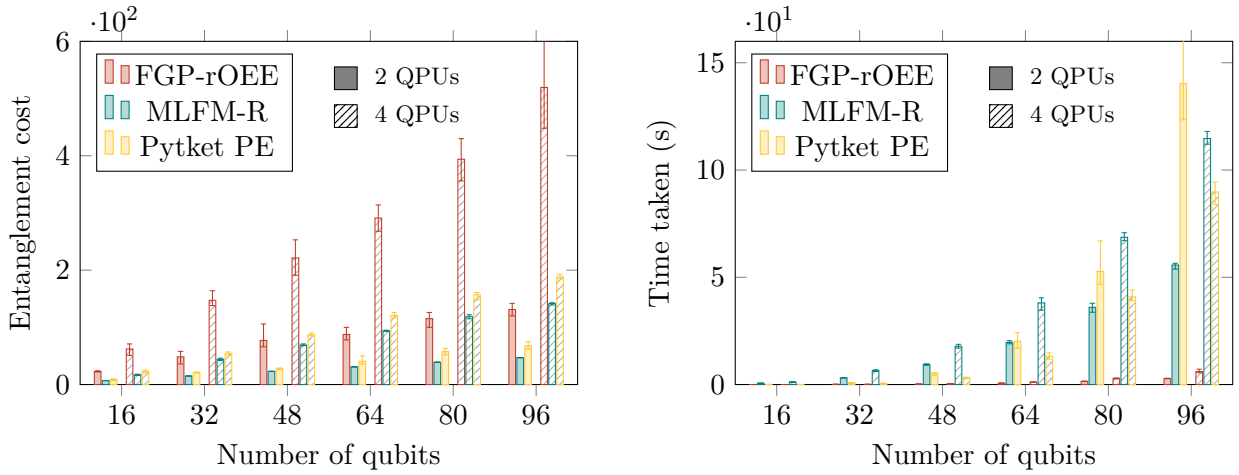


Figure 29: QAOA circuits partitioned over 2 and 4 QPUs.

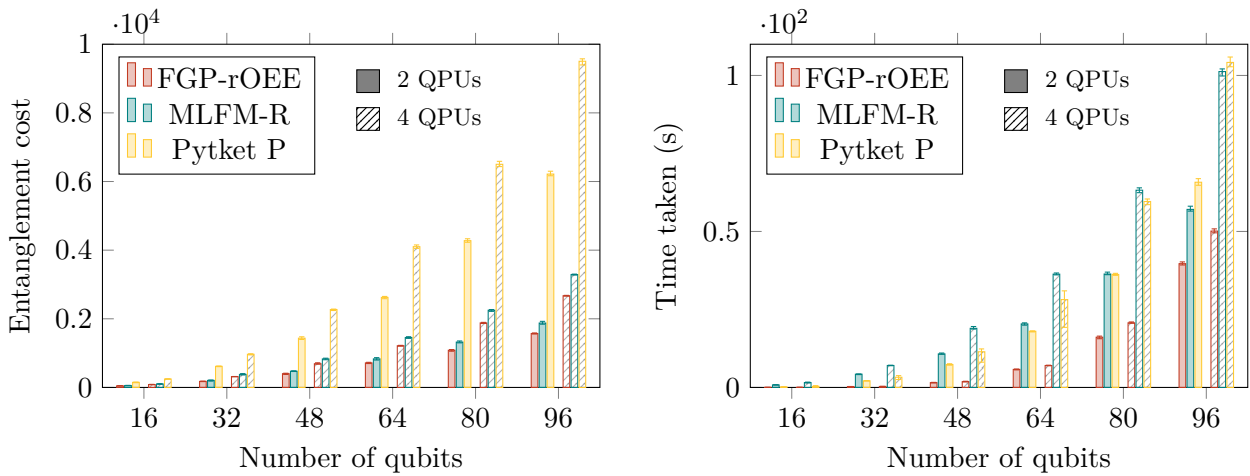


Figure 30: QV circuits, partitioned over 2 and 4 QPUs.

quantum circuit into a sequence of static graphs indicating the qubit interactions at each time-step, with time decaying contributions for future time-steps. A refinement heuristic is employed to achieve a fully-local partitioning for each time-step, using the assignment for each time-step as the starting point for the next. In similar fashion to GCP, the end result is a sequence of assignments of qubits to QPUs, one for each time-step of the circuit. The assignment guarantees that all two-qubit gates occur locally, using state teleportations to transition between each contiguous assignment. The algorithm used is referred to as FGP-rOEE. FGP-rOEE does not allow for gate teleportation or multi-gate teleportation, so typically underperforms in circuits which permit large groups of teleportation compatible groups.

8 Discussion

The results indicate that the proposed framework can achieve lower entanglement costs than existing, state-of-the-art techniques, provided that an appropriate algorithm is used to partition the resulting hypergraph. The results in Fig. 18 show the effectiveness of employing a gate grouping routine, allowing entanglement costs to be reduced via multi-gate teleportation. However, Fig. 19b highlights that this is traded off with the communication qubit capacity required to achieve these entanglement costs. While this means some architectures may be limited in the extent to which they can benefit from multi-gate teleportation, we believe that this should serve as an indication that large numbers of communication qubits are desirable for DQC architectures. Fig. 20 shows the effectiveness of using an exploratory variant of the FM algorithm which is more effec-

tive at escaping local minima. This is particularly important given the structure of the hypergraph, where using a static initial assignment of qubits to partitions initialises the algorithm in a local minimum 14. The exploratory variant allows larger sequences of moves to be probed, which may move the same node more than once, ultimately breaking into lower cost solution regions. Investigation of the multilevel framework shows that all coarsening strategies result in both lower entanglement costs and shorter runtime than the basic FM approach 21. The recursive coarsening strategy proves to be both the most effective and the most time efficient (when the number of nodes moved is not capped 21b), so is used as the main method for comparison with other techniques. Figs. 23, 24, 25 and 26 compare the recursive multilevel FM (MLFM-R) with two methods from Pytket-DQC (Partition and PartitionEmbed) and the FGP-rOEE algorithm from Ref. [23]. MLFM-R achieves the lowest entanglement costs for two-qubit gate proportions of 0.3 and 0.5, roughly matches the best performing methods for 0.7, though underperforms for 0.9. This is likely due to the fact that the Pytket-DQC methods optimise for detached gates, those which are executed in a partition which is not local to either the root or the receiver qubit. This is an effective technique for extremely high proportions of two-qubit gates. Since we do not consider this possibility, we limit the scope of multi-gate teleportation and thus aim to extend the generality of the framework in this way in future. In the time results, MLFM-R is significantly faster than Pytket ESD, but slower than Pytket PE and FGP-rOEE. This is primarily due to the fact that the core FM algorithm, in all cases, scales also with the number of partitions. In these tests, the number of QPUs is increased by one each time the number of qubits is increased, such that the time is scaling with both the circuit size and the number of partitions. This is a limitation that we aim to mitigate in the future. However, in Fig. 27 we show that, for a constant number of partitions (2 and 4), the MLFM-R outperforms even the fastest Pytket-DQC method, Partition, in both entanglement costs and time, as well as the FGP-rOEE algorithm. We were unable to complete these tests for Pytket PE or ESD, since the runtime was too long. This demonstrates that MLFM-R is able to scale to circuits with much

larger numbers of qubits when there is an appropriate limit on the number of partitions.

Furthermore, it is possible to reduce the time even further by terminating before the finest levels of refinement, though we do not investigate this here. In Fig. 28 we investigate the performance of the algorithm on QFT circuits. Interestingly, as mentioned in Sec. 7.1.2, we note that no improvement is achieved for any QFT circuits using any FM methods, though we achieve a very low entanglement cost. This indicates that the initial placement is a global optimum after the greedy gate grouping. In practice, it may not be necessary to perform any optimisation, and the initial placement can be used alongside the greedy gate grouping routine. For smaller QFT circuits, MLFM-R achieves the lowest costs, while for larger circuits, Pytket PE achieves the lowest costs. Additionally, large hyper-edges in QFT circuits leads to slow runtimes for MLFM-R. In practice however, we would not expect to use the FM algorithm for QFT circuits, since the greedy gate grouping pass is sufficient to achieve low entanglement costs. Fig. 29 displays the results generated from QAOA circuits, in which MLFM-R achieves the lowest entanglement costs. The time taken here is much longer than for FGP-rOEE, but predominantly shorter than Pytket PE, which displays erratic performance on these tests. The performance of the Pytket methods is very sensitive to the number of qubits, since the number of qubits is increased by one for each increase in circuit size. This means that the number of QPUs is also increased, which results in a large increase in the time taken. The MLFM-R method is able to scale to larger circuits than the other methods, since it does not require a static assignment of qubits to QPUs. The time taken for MLFM-R is significantly longer than for the other methods, but this is due to the fact that we are using a large number of partitions. In practice, we would expect to use fewer partitions, and thus achieve lower times. Fig. 30 shows the results for QV circuits. Previously, QV circuits were identified as difficult circuits to partition using only gate teleportation [55, 53], since they contain no potential for gate grouping. Consequently, methods such as FGP-rOEE, which use only state teleportation, are very effective at distributing QV circuits. The performance of the MLFM-R is comparable, but slower since the so-

Table 1: Overall comparison of MLFM-R and Pytket PE across all tests completed. We calculate a size independent metric for each circuit, where we divide the mean best e-bit cost achieved by the total number of two-qubit gates in each circuit, averaging over all circuits for each benchmark. A * indicates where we were unable to use Pytket PE due to runtime, so instead used P.

Circuit	Partitions	Ref.	E-bit Fraction	
			MLFM-R	PE
CP	2-12	[23,24,25,26]	0.418	0.413
CP-large*	2	[27]	0.213	0.257
CP-large*	4	[27]	0.394	0.457
QAOA	2	[29]	0.023	0.032
QAOA	4	[29]	0.065	0.085
QASM	2-4	[2]	0.049	0.098
QASM-large	2-4	[3]	0.023	0.054
QFT	2	[28]	0.023	0.028
QFT	4	[28]	0.064	0.065
QV*	2	[30]	0.136	0.419
QV*	4	[30]	0.241	0.66
Mean	N/A	N/A	0.15	0.233

lution space is much larger. From Pytket-DQC, we were only able to use Partition, since PartitionEmbed and EmbedSteinerDetached were too slow for QV circuits and showed no benefit over Partition at small scales. Finally, Tab. 2 and Tab. 3 shows results from the QASM benchmark suite circuits. For each circuit, we optimise the partitioning over 2, 3 and 4 QPUs. We summarise the comparison between MLFM-R and the next best performing method in Pytket-DQC in Tab. 1. Pytket EmbedSteinerDetached is too slow to run on many of the benchmarks, so we primarily compare with PartitionEmbed. However, in some cases, the embedding refinement was too slow and we had to use just Partition, which usually gives similar results and is significantly faster. These cases are indicated on the table. We use a size-independent metric, in which the optimised entanglement cost in terms of e-bit count is divided by the total number of qubits, giving the *e-bit fraction*. We do the same for the time taken. For the e-bit fraction, over all tests, we outperform the next best method by over 35%, which is significant. MLFM-R is often faster than PartitionEmbed, and is also faster than Partition for the large benchmarks (though Partition is faster in most other cases). FGP-rOEE is often the fastest method, but the limitation of only allowing state teleportation means that the entanglement costs are usually significantly higher, so we do not include the results in Tab. 1.

9 Conclusions

In this work, we have introduced and investigated a multilevel framework for partitioning quantum circuits over distributed quantum processing units. We formulated quantum circuit partitioning as a problem of partitioning temporally extended hypergraphs with a custom objective function, counting entanglement costs from quantum state teleportation, multi-gate teleportation and a new procedure termed *nested state teleportation*. The partitioning is based on the Fiduccia-Mattheyses algorithm – a well-known, efficient heuristic for hypergraph partitioning. We adapted the algorithm to fit the constraints of the problem and designed a unique objective corresponding to entanglement requirements. We illustrated how to efficiently incorporate this objective in the algorithm. We extended the framework to include temporal coarsening of problem hypergraphs, allowing us to partition at multiple levels of granularity. We demonstrated that multilevel partitioning can both reduce runtime and improve solution quality. We were able to significantly outperform state-of-the-art methods in terms of entanglement requirements. The results indicate that multilevel partitioning, coupled with a sufficiently general problem formulation, forms a highly effective framework for entanglement minimisation that should be integrated into future compiler stacks for distributed quan-

tum computing.

10 Future work

While the multilevel partitioning framework has proved to be very effective, there are a number of improvements still to be made. A limitation of the framework is that communication qubits are only accounted for in the final circuit extraction phase. This means that the algorithm may produce a partitioning which is not feasible due to a lack of communication qubits. We plan to introduce problem variants where we explicitly account for communication qubits available in the system, while also providing post-processing methods for mitigating communication qubit limitations. Additionally, techniques such as detached gates and embedding of non-local unitaries, identified and used in Refs. [18, 20, 55], could be incorporated into the framework to further reduce entanglement costs. Finally, we aim to extend the framework to consider general quantum networks, with limited connectivity and noisy hardware. We have avoided this in the current work, since the focus has been on the partitioning problem, but we believe that the framework can be extended to consider these limitations with careful consideration of entanglement swapping and purification requirements [67, 68]. We plan to include all extensions into the `disqco` library, with the hope of providing a complete framework for quantum circuit partitioning and distribution.

Acknowledgements

The authors acknowledge funding from the Engineering and Physical Sciences Research Council (EPSRC) funded Distributed Quantum Computing project, grant number EP/W032643/1.

References

- [1] Marcello Caleffi, Michele Amoretti, Davide Ferrari, Jessica Illiano, Antonio Manzalini, and Angela Sara Cacciapuoti. Distributed quantum computing: A survey. *Computer Networks*, 254: 110672, 2024. ISSN 1389-1286. DOI: <https://doi.org/10.1016/j.comnet.2024.110672>.
- [2] Nemanja Isailovic, Yatish Patel, Mark Whitney, and John Kubiawicz. Interconnection Networks for Scalable Quantum Computers. *ACM SIGARCH Computer Architecture News*, 34(2):366–377, May 2006. ISSN 0163-5964. DOI: [10.1145/1150019.1136505](https://doi.org/10.1145/1150019.1136505). URL <https://dl.acm.org/doi/10.1145/1150019.1136505>.
- [3] M. Akhtar, F. Bonus, F. R. Lebrun-Gallagher, N. I. Johnson, M. Siegele-Brown, S. Hong, S. J. Hile, S. A. Kulmiya, S. Weidt, and W. K. Hensinger. A high-fidelity quantum matter-link between ion-trap microchip modules. *Nature Communications*, 14(1):531, February 2023. ISSN 2041-1723. DOI: [10.1038/s41467-022-35285-3](https://doi.org/10.1038/s41467-022-35285-3). URL <https://www.nature.com/articles/s41467-022-35285-3>. Publisher: Nature Publishing Group.
- [4] V. Krutyanskiy, M. Galli, V. Krcmarsky, S. Baier, D. A. Fioretto, Y. Pu, A. Mazloom, P. Sekatski, M. Canteri, M. Teller, J. Schupp, J. Bate, M. Meraner, N. Sangouard, B. P. Lanyon, and T. E. Northup. Entanglement of trapped-ion qubits separated by 230 meters. *Phys. Rev. Lett.*, 130:050803, Feb 2023. DOI: [10.1103/PhysRevLett.130.050803](https://doi.org/10.1103/PhysRevLett.130.050803). URL <https://link.aps.org/doi/10.1103/PhysRevLett.130.050803>.
- [5] Jameson O’Reilly, George Toh, Isabella Goetting, Sagnik Saha, Mikhail Shalaev, Allison L. Carter, Andrew Risinger, Ashish Kalakuntla, Tingguang Li, Ashrit Verma, and Christopher Monroe. Fast photon-mediated entanglement of continuously cooled trapped ions for quantum networking. *Phys. Rev. Lett.*, 133:090802, Aug 2024. DOI: [10.1103/PhysRevLett.133.090802](https://doi.org/10.1103/PhysRevLett.133.090802). URL <https://link.aps.org/doi/10.1103/PhysRevLett.133.090802>.
- [6] Francis Afzal, Mohsen Akhlaghi, Stefanie J. Beale, Olinka Bedroya, Kristin Bell, Laurent Bergeron, Kent Bonsma-Fisher, Polina Bychkova, Zachary M. E. Chaisson, Camille Chartrand, Chloe Clear, Adam Darcie, Adam DeAbreu, Colby DeLisle, Lesley A. Duncan, Chad Dundas Smith, John Dunn,

- Amir Ebrahimi, Nathan Evetts, Daker Fernandes Pinheiro, Patricio Fuentes, Tristen Georgiou, Biswarup Guha, Rafael Haenel, Daniel Higginbottom, Daniel M. Jackson, Navid Jahed, Amin Khorshidahmad, Prasoon K. Shandilya, Alexander T. K. Kurkjian, Nikolai Lauk, Nicholas R. Lee-Hone, Eric Lin, Rostyslav Litynsky, Duncan Lock, Lisa Ma, Iain MacGilp, Evan R. MacQuarrie, Aaron Mar, Alireza Marefat Khah, Alex Matiash, Evan Meyer-Scott, Cathryn P. Michaels, Juliana Motira, Narwan Kabir Noori, Egor Ospadov, Ekta Patel, Alexander Patscheider, Danny Paulson, Ariel Petruk, Adarsh L. Ravindranath, Bogdan Reznychenko, Myles Ruether, Jeremy Ruscica, Kunal Saxena, Zachary Schaller, Alex Seidlitz, John Senger, Youn Seok Lee, Orbel Sevoyan, Stephanie Simmons, Oney Soykal, Leea Stott, Quyen Tran, Spyros Tserkis, Ata Ulhaq, Wyatt Vine, Russ Weeks, Gary Wolfowicz, and Isao Yoneda. Distributed quantum computing in silicon, 2024. URL <https://arxiv.org/abs/2406.01704>.
- [7] Aziza Almanakly, Beatriz Yankelevich, Max Hays, Bharath Kannan, Réouven Assouly, Alex Greene, Michael Gingras, Bethany M. Niedzielski, Hannah Stickler, Mollie E. Schwartz, Kyle Serniak, Joel \hat{I} -j Wang, Terry P. Orlando, Simon Gustavsson, Jeffrey A. Grover, and William D. Oliver. Deterministic remote entanglement using a chiral quantum interconnect. *Nature Physics*, pages 1–6, March 2025. ISSN 1745-2481. DOI: [10.1038/s41567-025-02811-1](https://doi.org/10.1038/s41567-025-02811-1). URL <https://www.nature.com/articles/s41567-025-02811-1>. Publisher: Nature Publishing Group.
- [8] Sagnik Saha, Mikhail Shalaev, Jameson O’Reilly, Isabella Goetting, George Toh, Ashish Kalakuntla, Yichao Yu, and Christopher Monroe. High-fidelity remote entanglement of trapped atoms mediated by time-bin photons. *Nature Communications*, 16(1):2533, March 2025. ISSN 2041-1723. DOI: [10.1038/s41467-025-57557-4](https://doi.org/10.1038/s41467-025-57557-4). URL <https://www.nature.com/articles/s41467-025-57557-4>. Publisher: Nature Publishing Group.
- [9] Kevin S. Chou, Jacob Z. Blumoff, Christopher S. Wang, Philip C. Reinhold, Christopher J. Axline, Yvonne Y. Gao, L. Frunzio, M. H. Devoret, Liang Jiang, and R. J. Schoelkopf. Deterministic teleportation of a quantum gate between two logical qubits. *Nature*, 561(7723):368–373, September 2018. ISSN 1476-4687. DOI: [10.1038/s41586-018-0470-y](https://doi.org/10.1038/s41586-018-0470-y). URL <https://www.nature.com/articles/s41586-018-0470-y>. Publisher: Nature Publishing Group.
- [10] Yong Wan, Daniel Kienzler, Stephen D. Erickson, Karl H. Mayer, Ting Rei Tan, Jenny J. Wu, Hilma M. Vasconcelos, Scott Glancy, Emanuel Knill, David J. Wineland, Andrew C. Wilson, and Dietrich Leibfried. Quantum gate teleportation between separated qubits in a trapped-ion processor. *Science*, 364(6443):875–878, 2019. DOI: [10.1126/science.aaw9415](https://doi.org/10.1126/science.aaw9415). URL <https://www.science.org/doi/abs/10.1126/science.aaw9415>.
- [11] D. Main, P. Drmota, D. P. Nadlinger, E. M. Ainley, A. Agrawal, B. C. Nichol, R. Srinivas, G. Araneda, and D. M. Lucas. Distributed quantum computing across an optical network link. *Nature*, 638(8050):383–388, February 2025. ISSN 1476-4687. DOI: [10.1038/s41586-024-08404-x](https://doi.org/10.1038/s41586-024-08404-x). URL <https://doi.org/10.1038/s41586-024-08404-x>.
- [12] James Ang, Gabriella Carini, Yanzhu Chen, Isaac Chuang, Michael Demarco, Sophia Economou, Alec Eickbusch, Andrei Faraon, Kai-Mei Fu, Steven Girvin, Michael Hatridge, Andrew Houck, Paul Hilaire, Kevin Krsulich, Ang Li, Chenxu Liu, Yuan Liu, Margaret Martonosi, David McKay, Jim Misewich, Mark Ritter, Robert Schoelkopf, Samuel Stein, Sara Sussman, Hong Tang, Wei Tang, Teague Tomesh, Norm Tubman, Chen Wang, Nathan Wiebe, Yongxin Yao, Dillon Yost, and Yiyu Zhou. Arquin: Architectures for multinode superconducting quantum computers. *ACM Transactions on Quantum Computing*, 5(3), September 2024. DOI: [10.1145/3674151](https://doi.org/10.1145/3674151). URL <https://doi.org/10.1145/3674151>.
- [13] David Barral, F. Javier Cardama, Guillermo Díaz, Daniel Faílde, Iago F. Llovo, Mariamo Mussa Juane, Jorge Vázquez-Pérez, Juan Villasuso, César Piñeiro, Natalia

- Costas, Juan C. Pichel, Tomás F. Pena, and Andrés Gómez. Review of Distributed Quantum Computing. From single QPU to High Performance Quantum Computing, 2024. URL <https://arxiv.org/abs/2404.01265>. arXiv:2404.01265 [quant-ph].
- [14] Mariam Zomorodi-Moghadam, Mahboobeh Houshmand, and Monireh Houshmand. Optimizing Teleportation Cost in Distributed Quantum Circuits. *International Journal of Theoretical Physics*, 57(3):848–861, March 2018. ISSN 1572-9575. DOI: [10.1007/s10773-017-3618-x](https://doi.org/10.1007/s10773-017-3618-x). URL <https://doi.org/10.1007/s10773-017-3618-x>.
- [15] Omid Daei, Keivan Navi, and Mariam Zomorodi-Moghadam. Optimized Quantum Circuit Partitioning. *International Journal of Theoretical Physics*, 59(12):3804–3820, December 2020. ISSN 0020-7748, 1572-9575. DOI: [10.1007/s10773-020-04633-8](https://doi.org/10.1007/s10773-020-04633-8). URL <http://link.springer.com/10.1007/s10773-020-04633-8>.
- [16] Davood Dadkhah, Mariam Zomorodi, and Seyed Ebrahim Hosseini. A New Approach for Optimization of Distributed Quantum Circuits. *International Journal of Theoretical Physics*, 60(9):3271–3285, September 2021. ISSN 1572-9575. DOI: [10.1007/s10773-021-04904-y](https://doi.org/10.1007/s10773-021-04904-y). URL <https://doi.org/10.1007/s10773-021-04904-y>.
- [17] Davide Ferrari, Angela Sara Cacciapuoti, Michele Amoretti, and Marcello Caleffi. Compiler Design for Distributed Quantum Computing. *IEEE Transactions on Quantum Engineering*, 2:1–20, 2021. ISSN 2689-1808. DOI: [10.1109/TQE.2021.3053921](https://doi.org/10.1109/TQE.2021.3053921). URL <https://ieeexplore.ieee.org/document/9334411/>.
- [18] Ranjani G Sundaram. Efficient Distribution of Quantum Circuits, 2021.
- [19] Eesa Nikahd, Naser Mohammadzadeh, Mehdi Sedighi, and Morteza Saheb Zamani. Automated window-based partitioning of quantum circuits. *Physica Scripta*, 96(3):035102, January 2021. ISSN 1402-4896. DOI: [10.1088/1402-4896/abd57c](https://doi.org/10.1088/1402-4896/abd57c). URL <https://dx.doi.org/10.1088/1402-4896/abd57c>. Publisher: IOP Publishing.
- [20] Jun-Yi Wu, Kosuke Matsui, Tim Forrer, Akihito Soeda, Pablo Andrés-Martínez, Daniel Mills, Luciana Henaut, and Mio Murao. Entanglement-efficient bipartite-distributed quantum computing. *Quantum*, 7:1196, December 2023. DOI: [10.22331/q-2023-12-05-1196](https://doi.org/10.22331/q-2023-12-05-1196). URL <https://quantum-journal.org/papers/q-2023-12-05-1196/>. Publisher: Verein zur Förderung des Open Access Publizierens in den Quantenwissenschaften.
- [21] Anbang Wu, Hezi Zhang, Gushu Li, Alireza Shabani, Yuan Xie, and Yufei Ding. AutoComm: A Framework for Enabling Efficient Communication in Distributed Quantum Programs. In *2022 55th IEEE/ACM International Symposium on Microarchitecture (MICRO)*, pages 1027–1041, Chicago, IL, USA, October 2022. IEEE. ISBN 978-1-66546-272-3. DOI: [10.1109/MICRO56248.2022.00074](https://doi.org/10.1109/MICRO56248.2022.00074). URL <https://ieeexplore.ieee.org/document/9923799/>.
- [22] Anbang Wu, Yufei Ding, and Ang Li. QuComm: Optimizing Collective Communication for Distributed Quantum Computing. In *Proceedings of the 56th Annual IEEE/ACM International Symposium on Microarchitecture, MICRO '23*, pages 479–493, New York, NY, USA, December 2023. Association for Computing Machinery. ISBN 9798400703294. DOI: [10.1145/3613424.3614253](https://doi.org/10.1145/3613424.3614253). URL <https://dl.acm.org/doi/10.1145/3613424.3614253>.
- [23] Jonathan M. Baker, Casey Duckering, Alexander Hoover, and Frederic T. Chong. Time-Sliced Quantum Circuit Partitioning for Modular Architectures, May 2020. URL <https://arxiv.org/abs/2005.12259v1>.
- [24] Daniele Cuomo, Marcello Caleffi, Kevin Kruslich, Filippo Tramonto, Gabriele Agliardi, Enrico Prati, and Angela Sara Cacciapuoti. Optimized Compiler for Distributed Quantum Computing. *ACM Transactions on Quantum Computing*, 4(2):1–29, June 2023. ISSN 2643-6809, 2643-6817. DOI: [10.1145/3579367](https://doi.org/10.1145/3579367). URL <https://dl.acm.org/doi/10.1145/3579367>.
- [25] Davide Ferrari, Stefano Carretta, and Michele Amoretti. A Modular Quantum Compilation Framework for Dis-

- tributed Quantum Computing. *IEEE Transactions on Quantum Engineering*, 4:1–13, 2023. ISSN 2689-1808. DOI: [10.1109/TQE.2023.3303935](https://doi.org/10.1109/TQE.2023.3303935). URL <https://ieeexplore.ieee.org/document/10214316/>.
- [26] Oliver Crampton, Panagiotis Promponas, Richard Chen, Paul Polakos, Leandros Tassioulas, and Louis Samuel. A Genetic Approach to Minimising Gate and Qubit Teleportations for Multi-Processor Quantum Circuit Distribution, May 2024. URL <http://arxiv.org/abs/2405.05875>. arXiv:2405.05875 [quant-ph].
- [27] Panagiotis Promponas, Akrit Mudvari, Luca Della Chiesa, Paul Polakos, Louis Samuel, and Leandros Tassioulas. Compiler for Distributed Quantum Computing: a Reinforcement Learning Approach, April 2024. URL <http://arxiv.org/abs/2404.17077>. arXiv:2404.17077 [quant-ph].
- [28] Xinyu Chen, Zilu Chen, Xueyun Cheng, and Zhijin Guan. Circuit Partitioning and Transmission Cost Optimization in Distributed Quantum Computing, September 2024. URL <http://arxiv.org/abs/2407.05953>. arXiv:2407.05953.
- [29] Eneet Kaur, Hassan Shapourian, Jiapeng Zhao, Michael Kilzer, Ramana Kompella, and Reza Nejabati. Optimized quantum circuit partitioning across multiple quantum processors, 2025. URL <https://arxiv.org/abs/2501.14947>.
- [30] Yingling Mao, Yu Liu, and Yuanyuan Yang. Qubit allocation for distributed quantum computing. In *IEEE INFOCOM 2023 - IEEE Conference on Computer Communications*, pages 1–10, 2023. DOI: [10.1109/INFOCOM53939.2023.10228915](https://doi.org/10.1109/INFOCOM53939.2023.10228915).
- [31] B. W. Kernighan and S. Lin. An efficient heuristic procedure for partitioning graphs. *The Bell System Technical Journal*, 49(2): 291–307, February 1970. ISSN 0005-8580. DOI: [10.1002/j.1538-7305.1970.tb01770.x](https://doi.org/10.1002/j.1538-7305.1970.tb01770.x). URL <https://ieeexplore.ieee.org/document/6771089>. Conference Name: The Bell System Technical Journal.
- [32] C.M. Fiduccia and R.M. Mattheyses. A linear-time heuristic for improving network partitions. In *19th Design Automation Conference*, pages 175–181, 1982. DOI: [10.1109/DAC.1982.1585498](https://doi.org/10.1109/DAC.1982.1585498).
- [33] L.A. Sanchis. Multiple-way network partitioning. *IEEE Transactions on Computers*, 38(1):62–81, January 1989. ISSN 1557-9956. DOI: [10.1109/12.8730](https://doi.org/10.1109/12.8730). URL <https://ieeexplore.ieee.org/document/8730>. Conference Name: IEEE Transactions on Computers.
- [34] Jason Cong and M’Lissa Smith. A parallel bottom-up clustering algorithm with applications to circuit partitioning in VLSI design. In *Proceedings of the 30th international on Design automation conference - DAC ’93*, pages 755–760, Dallas, Texas, United States, 1993. ACM Press. ISBN 978-0-89791-577-9. DOI: [10.1145/157485.165119](https://doi.org/10.1145/157485.165119). URL <http://portal.acm.org/citation.cfm?doid=157485.165119>.
- [35] Frank M. Johannes. Partitioning of VLSI circuits and systems. In *Proceedings of the 33rd annual conference on Design automation conference - DAC ’96*, pages 83–87, Las Vegas, Nevada, United States, 1996. ACM Press. ISBN 978-0-89791-779-7. DOI: [10.1145/240518.240535](https://doi.org/10.1145/240518.240535). URL <http://portal.acm.org/citation.cfm?doid=240518.240535>.
- [36] Dennis J.-H. Huang and Andrew B. Kahng. Partitioning-based standard-cell global placement with an exact objective. In *Proceedings of the 1997 international symposium on Physical design, ISPD ’97*, pages 18–25, New York, NY, USA, April 1997. Association for Computing Machinery. ISBN 978-0-89791-927-2. DOI: [10.1145/267665.267674](https://doi.org/10.1145/267665.267674). URL <https://dl.acm.org/doi/10.1145/267665.267674>.
- [37] George Karypis, Rajat Aggarwal, Vipin Kumar, and Shashi Shekhar. Multilevel hypergraph partitioning: application in VLSI domain. In *Proceedings of the 34th annual Design Automation Conference, DAC ’97*, pages 526–529, New York, NY, USA, June 1997. Association for Computing Machinery. ISBN 978-0-89791-920-3. DOI: [10.1145/266021.266273](https://doi.org/10.1145/266021.266273). URL <https://dl.acm.org/doi/10.1145/266021.266273>.
- [38] George Karypis and Vipin Kumar. A Fast and High Quality Multilevel Scheme for Partitioning Irregular Graphs. *SIAM Jour-*

- nal on Scientific Computing*, 20(1):359–392, January 1998. ISSN 1064-8275, 1095-7197. DOI: [10.1137/S1064827595287997](https://doi.org/10.1137/S1064827595287997). URL <http://epubs.siam.org/doi/10.1137/S1064827595287997>.
- [39] Henning Meyerhenke, Peter Sanders, and Christian Schulz. Partitioning Complex Networks via Size-constrained Clustering, March 2014. URL <http://arxiv.org/abs/1402.3281>. arXiv:1402.3281 [cs].
- [40] Sebastian Schlag, Tobias Heuer, Lars Gottesbüren, Yaroslav Akhremtsev, Christian Schulz, and Peter Sanders. High-Quality Hypergraph Partitioning, June 2021. URL <http://arxiv.org/abs/2106.08696>. arXiv:2106.08696 [cs].
- [41] Tianyi Peng, Aram Harrow, Maris Ozols, and Xiaodi Wu. Simulating Large Quantum Circuits on a Small Quantum Computer. *Physical Review Letters*, 125(15):150504, October 2020. ISSN 0031-9007, 1079-7114. DOI: [10.1103/PhysRevLett.125.150504](https://doi.org/10.1103/PhysRevLett.125.150504). URL <http://arxiv.org/abs/1904.00102>. arXiv:1904.00102 [quant-ph].
- [42] Wei Tang, Teague Tomesh, Martin Suchara, Jeffrey Larson, and Margaret Martonosi. CutQC: using small Quantum computers for large Quantum circuit evaluations. In *Proceedings of the 26th ACM International Conference on Architectural Support for Programming Languages and Operating Systems*, ASPLOS '21, pages 473–486, New York, NY, USA, April 2021. Association for Computing Machinery. ISBN 978-1-4503-8317-2. DOI: [10.1145/3445814.3446758](https://doi.org/10.1145/3445814.3446758). URL <https://dl.acm.org/doi/10.1145/3445814.3446758>.
- [43] Wei Tang and Margaret Martonosi. Cutting Quantum Circuits to Run on Quantum and Classical Platforms, May 2022. URL <http://arxiv.org/abs/2205.05836>. arXiv:2205.05836 [quant-ph].
- [44] Saikat Basu, Arnav Das, Amit Saha, Amlan Chakrabarti, and Susmita Sur-Kolay. FragQC: An Efficient Quantum Error Reduction Technique using Quantum Circuit Fragmentation, September 2023. URL <http://arxiv.org/abs/2310.00444>. arXiv:2310.00444 [quant-ph].
- [45] Teague Tomesh, Zain H. Saleem, Michael A. Perlin, Pranav Gokhale, Martin Suchara, and Margaret Martonosi. Divide and Conquer for Combinatorial Optimization and Distributed Quantum Computation, October 2023. URL <http://arxiv.org/abs/2107.07532>. arXiv:2107.07532 [quant-ph].
- [46] Marvin Bechtold, Johanna Barzen, Frank Leymann, Alexander Mandl, Julian Obst, Felix Truger, and Benjamin Weder. Investigating the effect of circuit cutting in QAOA for the MaxCut problem on NISQ devices. *Quantum Science and Technology*, 8(4):045022, October 2023. ISSN 2058-9565. DOI: [10.1088/2058-9565/acf59c](https://doi.org/10.1088/2058-9565/acf59c). URL <http://arxiv.org/abs/2302.01792>. arXiv:2302.01792 [quant-ph].
- [47] Turbasu Chatterjee, Arnav Das, Shah Ishmam Mohtashim, Amit Saha, and Amlan Chakrabarti. Qurzon: A Prototype for a Divide and Conquer-Based Quantum Compiler for Distributed Quantum Systems. *SN Computer Science*, 3(4):323, June 2022. ISSN 2661-8907. DOI: [10.1007/s42979-022-01207-9](https://doi.org/10.1007/s42979-022-01207-9). URL <https://doi.org/10.1007/s42979-022-01207-9>.
- [48] David P. DiVincenzo. The physical implementation of quantum computation. *Fortschritte der Physik*, 48(9–11):771–783, September 2000. ISSN 1521-3978. DOI: [10.1002/1521-3978\(200009\)48:9/11<771::aid-prop771>3.0.co;2-e](https://doi.org/10.1002/1521-3978(200009)48:9/11<771::aid-prop771>3.0.co;2-e). URL [http://dx.doi.org/10.1002/1521-3978\(200009\)48:9/11<771::AID-PROP771>3.0.CO;2-E](http://dx.doi.org/10.1002/1521-3978(200009)48:9/11<771::AID-PROP771>3.0.CO;2-E).
- [49] Charles H. Bennett, Gilles Brassard, Claude Crépeau, Richard Jozsa, Asher Peres, and William K. Wootters. Teleporting an unknown quantum state via dual classical and Einstein-Podolsky-Rosen channels. *Physical Review Letters*, 70(13):1895–1899, March 1993. DOI: [10.1103/PhysRevLett.70.1895](https://doi.org/10.1103/PhysRevLett.70.1895). URL <https://link.aps.org/doi/10.1103/PhysRevLett.70.1895>. Publisher: American Physical Society.
- [50] Daniel Gottesman and Isaac L. Chuang. Demonstrating the viability of universal quantum computation using teleportation and single-qubit operations. *Nature*, 402(6760):390–393, November 1999. ISSN 1476-4687. DOI: [10.1038/46503](https://doi.org/10.1038/46503). URL <https://www.nature.com/articles/46503>. Pub-

- lisher: Nature Publishing Group.
- [51] J. Eisert, K. Jacobs, P. Papadopoulos, and M. B. Plenio. Optimal local implementation of nonlocal quantum gates. *Physical Review A*, 62(5):052317, October 2000. DOI: [10.1103/PhysRevA.62.052317](https://doi.org/10.1103/PhysRevA.62.052317). URL <https://link.aps.org/doi/10.1103/PhysRevA.62.052317>. Publisher: American Physical Society.
- [52] Anocha Yimsiriwattana and Samuel J. Lomonaco Jr. Generalized GHZ States and Distributed Quantum Computing, March 2004. URL <http://arxiv.org/abs/quant-ph/0402148>. arXiv:quant-ph/0402148.
- [53] Felix Burt, Kuan-Cheng Chen, and Kin K. Leung. Generalised circuit partitioning for distributed quantum computing. In *2024 IEEE International Conference on Quantum Computing and Engineering (QCE)*, volume 02, pages 173–178, 2024. DOI: [10.1109/QCE60285.2024.10273](https://doi.org/10.1109/QCE60285.2024.10273).
- [54] Anocha Yimsiriwattana and Samuel J. Lomonaco Jr. Distributed quantum computing: a distributed Shor algorithm, August 2004. URL <http://proceedings.spiedigitallibrary.org/proceeding.aspx?doi=10.1117/12.546504>.
- [55] Pablo Andres-Martinez, Tim Forrer, Daniel Mills, Jun-Yi Wu, Luciana Henaut, Kentaro Yamamoto, Mio Murao, and Ross Duncan. Distributing circuits over heterogeneous, modular quantum computing network architectures. *Quantum Science and Technology*, 9(4):045021, aug 2024. DOI: [10.1088/2058-9565/ad6734](https://doi.org/10.1088/2058-9565/ad6734). URL <https://dx.doi.org/10.1088/2058-9565/ad6734>.
- [56] Pablo Andrés-Martínez and Chris Heunen. Automated distribution of quantum circuits via hypergraph partitioning. *Physical Review A*, 100(3):032308, September 2019. DOI: [10.1103/PhysRevA.100.032308](https://doi.org/10.1103/PhysRevA.100.032308). URL <https://link.aps.org/doi/10.1103/PhysRevA.100.032308>. Publisher: American Physical Society.
- [57] Ranjani G. Sundaram, Himanshu Gupta, and C. R. Ramakrishnan. Distribution of Quantum Circuits Over General Quantum Networks, June 2022. URL <http://arxiv.org/abs/2206.06437>. arXiv:2206.06437 [quant-ph].
- [58] Felix Burt. Disqco, 2025. URL <https://github.com/felix-burt/DISQCO>.
- [59] Ranjani G. Sundaram, Himanshu Gupta, and C. R. Ramakrishnan. Efficient distribution of quantum circuits. In *International Symposium on Distributed Computing*, 2021. URL <https://api.semanticscholar.org/CorpusID:238359852>.
- [60] Hyunho Cha and Jungwoo Lee. Module-conditioned distribution of quantum circuits, January 2025. URL <http://arxiv.org/abs/2501.11816>. arXiv:2501.11816 [quant-ph].
- [61] Andrew W. Cross, Lev S. Bishop, Sarah Sheldon, Paul D. Nation, and Jay M. Gambetta. Validating quantum computers using randomized model circuits. *Physical Review A*, 100(3):032328, September 2019. ISSN 2469-9926, 2469-9934. DOI: [10.1103/PhysRevA.100.032328](https://doi.org/10.1103/PhysRevA.100.032328). URL <http://arxiv.org/abs/1811.12926>. arXiv:1811.12926 [quant-ph].
- [62] Edward Farhi, Jeffrey Goldstone, and Sam Gutmann. A Quantum Approximate Optimization Algorithm, November 2014. URL <http://arxiv.org/abs/1411.4028>. arXiv:1411.4028 [quant-ph].
- [63] Ang Li, Samuel Stein, Sriram Krishnamoorthy, and James Ang. Qasm-bench: A low-level qasm benchmark suite for nisq evaluation and simulation, 2022. URL <https://arxiv.org/abs/2005.13018>.
- [64] Pablo Andres-Martinez, Daniel Mills, Tim Forrer, and Luciana Henaut. CQCL/pytket-dqc, June 2024. URL <https://github.com/CQCL/pytket-dqc>. original-date: 2021-12-20T18:54:45Z.
- [65] Pablo Andres-Martinez, Tim Forrer, Daniel Mills, Jun-Yi Wu, Luciana Henaut, Kentaro Yamamoto, Mio Murao, and Ross Duncan. Distributing circuits over heterogeneous, modular quantum computing network architectures. *Quantum Science and Technology*, 9(4):045021, August 2024. ISSN 2058-9565. DOI: [10.1088/2058-9565/ad6734](https://doi.org/10.1088/2058-9565/ad6734). URL <https://dx.doi.org/10.1088/2058-9565/ad6734>. Publisher: IOP Publishing.
- [66] Seyon Sivarajah, Silas Dilkes, Alexander Cowtan, Will Simmons, Alec Edgington, and Ross Duncan. $t|ket\rangle$: a retargetable com-

pilers for nisq devices. *Quantum Science and Technology*, 6(1):014003, nov 2020. DOI: [10.1088/2058-9565/ab8e92](https://doi.org/10.1088/2058-9565/ab8e92). URL <https://dx.doi.org/10.1088/2058-9565/ab8e92>.

- [67] Charles H. Bennett, Gilles Brassard, Sandu Popescu, Benjamin Schumacher, John A. Smolin, and William K. Wootters. Purification of Noisy Entanglement and Faithful Teleportation via Noisy Channels. *Physical Review Letters*, 76(5):722–725, January 1996. DOI: [10.1103/PhysRevLett.76.722](https://doi.org/10.1103/PhysRevLett.76.722). URL <https://link.aps.org/doi/10.1103/PhysRevLett.76.722>. Publisher: American Physical Society.
- [68] H.-J. Briegel, W. Dür, J. I. Cirac, and P. Zoller. Quantum repeaters for communication, March 1998. URL <http://arxiv.org/abs/quant-ph/9803056>. arXiv:quant-ph/9803056.

A QASM results tables

In Tab. 2 and Tab. 3, we show the results of the QASM benchmark suite circuits, partitioned over 2, 3 and 4 QPUs. The results are generated using the exploratory MLFM-R algorithm with a cap of n_q on the number of nodes moved per pass, for 10 passes, as for other results. Note that we transpile circuits into the U, CP gate set before partitioning. We test circuits from the *larger* section of the benchmark suite, though omit circuits of depth greater than 1000 after transpilation. Additionally, we omit QFT, QAOA and QV circuits, since they have already been tested.

A.1 FM auxiliary functions

Algorithm 5: Initial Routines for FM

```

Cost( $H, \Phi, COSTS$ ) Calculate total cost of
graph  $H$  under current assignment  $\Phi$ .
   $Cost \leftarrow 0$ ;
  foreach hyperedge  $e \in H$  do
     $Cost$ 
     $\leftarrow Cost + \text{EdgeCost}(e, \Phi, COSTS)$ ;
  return  $Cost$ ;

Gain( $v, p, \Phi, COSTS$ );
  // Gain( $v, p, \Phi, COSTS$ )
 $\Phi' \leftarrow \text{MoveNode}(\Phi, v, p)$ ;
 $gain \leftarrow 0$ ;
foreach hyperedge  $e \in H$  containing  $v$ 
do
   $eCost \leftarrow$ 
  RetrieveEdgeCost( $v, \Phi, COSTS$ );
   $newCost \leftarrow$ 
   $eCost - \text{EdgeCost}(e, \Phi', COSTS)$ ;
   $gain \leftarrow gain + newCost$ ;
return  $gain$ ;

BuildGainBuckets( $H, \Phi, K, COSTS$ );
  // BuildGainBuckets( $H, \Phi, K, COSTS$ )
GAINS  $\leftarrow$ 
  ComputeAllGains( $H, \Phi, K, COSTS$ );
BUCKETS  $\leftarrow \{\}$ ;
foreach ( $v, p$ ) where GAINS[ $v, p$ ]  $\neq -\infty$ 
do
   $g \leftarrow \text{GAINS}[v, p]$ ;
  BUCKETS[ $g$ ].add( $v, p$ );
return BUCKETS;

```

Here we include the auxiliary functions used

Algorithm 6: Auxiliary routines for FM-GCP

```

BestMove( $BUCKETS, LOCK, CAP, \Phi$ )for
  each gain descending do // gain from
  max to min in BUCKETS
  while BUCKETS[ $gain$ ]  $\neq \emptyset$  do
    ( $v^*, p^*$ )  $\leftarrow$ 
    ChooseRandom(BUCKETS[ $gain$ ]);
    BUCKETS[ $gain$ ].remove( $v^*, p^*$ );
  return None

MoveNode( $\Phi, v, p$ );
  // MoveNode( $\Phi, v, p$ )
 $\Phi'(x) \leftarrow \Phi(x) \ \forall x \neq v$ ;
 $\Phi'(v) \leftarrow p$ ;
return  $\Phi'$ ;

UpdateGains( $H, GAINS, BUCKETS, v^*, p^*, \Phi, COSTS$ )
Moves  $\leftarrow \{\}$ ;
foreach edge  $e \in A(v^*)$  do
  foreach  $u \in e$  with  $u \notin LOCK$  do
    for  $p \leftarrow 0$  to  $K - 1$  do
       $\delta_{u,p} \leftarrow$ 
      DeltaGainContrib( $u, e, p, c_e(\Phi), c_e(\Phi'), COSTS$ );
       $\Delta_{u,p} \leftarrow \Delta_{u,p} + \delta_{u,p}$ ;
      Moves.add( $u, p$ );
  foreach ( $u, p$ )  $\in$  Moves do
    BUCKETS[GAINS[ $u, p$ ]].remove( $u, p$ );
    GAINS[ $u, p$ ]  $\leftarrow \Delta_{u,p}$ ;
    BUCKETS[GAINS[ $u, p$ ]].add( $u, p$ );

```

in the FM algorithm. Alg. 5 contains functions used for initialising the main algorithm, creating the initial gain structures. Alg. 6 contains functions used for updating the gain structures, moving nodes and updating the cost. The main function in the initialisation is BUILDGAINBUCKETS, in which we calculate the gain for moving each node to each external partition, and then sort all the resulting moves into buckets corresponding to each gain value. Alg. 6 contains the sub-routines for choosing the best moves at each iteration, as well as the UPDATEGAINS function, which is the bulk of the computation in the main FM algorithm. The update gains function works by iterating over the edges in which the moved node is involved, since only these edges are affected by the move. The alternative would be to find the neighbours of the moved node and di-

Table 2: Comparison of entanglement cost and time taken for QASM benchmark suite circuits.

Circuit	Partitions	P Cost	P Time	PE Cost	PE Time	ESD Cost	ESD Time	MLFM-R Cost	MLFM-R Time
adder28	2	4	0.079	3.6	0.205	3	0.699	2.6	3.244
adder28	3	2	0.07	2	0.118	5	0.712	2	4.126
adder28	4	12	0.08	10.8	0.226	9	0.694	8.2	5.617
bv30	2	1	0.008	1	0.01	1	0.02	2	0.387
bv30	3	2	0.01	2	0.011	2	0.02	5.8	0.522
bv30	4	2.6	0.011	2.6	0.013	3	0.023	7.8	0.729
knn31	2	2.4	0.049	2.4	0.075	4	0.719	1	2.175
knn31	3	4.4	0.066	4.4	0.093	5	0.429	2	4.004
knn31	4	10.8	0.098	10.8	0.127	21	0.643	3	4.743
cc32	2	1	0.008	1	0.012	1	0.034	2.8	2.058
cc32	3	2.2	0.018	2.2	0.022	2	0.031	9.4	2.724
cc32	4	3	0.013	3	0.016	3	0.033	12.2	3.642
dnn33	2	4	0.095	4	0.179	4	1.115	4.2	3.093
dnn33	3	11	0.107	11	0.201	11	0.987	8.2	4.47
dnn33	4	28.8	0.221	28.8	0.318	36	1.111	12.6	6.516
ising34	2	1	0.023	1	0.034	1	0.111	1	0.123
ising34	3	6.6	0.03	6.6	0.042	9	0.116	2	0.173
ising34	4	13.4	0.035	13.4	0.049	17	0.124	3	0.246
cat35	2	1	0.01	1	0.014	1	0.025	1	1.048
cat35	3	9	0.028	9	0.032	25	0.045	2	1.411
cat35	4	9	0.027	9	0.032	23	0.045	3	1.952
wstate36	2	2	0.028	2	0.039	2	0.119	1.4	1.164
wstate36	3	4	0.033	4	0.044	4	0.124	2.6	1.562
wstate36	4	6	0.036	6	0.047	6	0.129	5	2.224
qugan39	2	5	0.121	5	0.233	5	2.092	3.4	3.662
qugan39	3	12	0.13	12	0.255	12	1.901	8	6.061
qugan39	4	22.6	0.169	21.6	0.448	21	1.764	14.2	7.338
ghz40	2	1	0.012	1	0.017	1	0.032	1	1.38
ghz40	3	4.4	0.023	4.4	0.028	14	0.045	2	1.877
ghz40	4	3	0.017	3	0.022	3	0.037	3	2.579
knn41	2	1	0.073	1	0.118	1	2.044	1	5.192
knn41	3	5	0.092	5	0.14	5	1.252	2	6.84
knn41	4	10.8	0.159	10.8	0.209	15	0.94	3	10.87
swaptest41	2	1	0.07	1	0.113	1	2.021	1	5.199
swaptest41	3	5	0.089	5	0.135	5	1.233	2	6.496
swaptest41	4	9.2	0.125	9.2	0.173	15	0.904	3	11.027
ising42	2	1	0.031	1	0.048	1	0.176	1	0.154
ising42	3	2	0.035	2	0.053	2	0.182	2	0.218
ising42	4	14.4	0.049	14.4	0.068	19	0.184	3	0.298

Table 3: Comparison of entanglement cost and time taken for larger QASM benchmark suite circuits.

Circuit	Partitions	P Cost	P Time	PE Cost	PE Time	ESD Cost	ESD Time	MLFM-R Cost	MLFM-R Time
dnn51	2	4	0.199	4	0.395	4	5.024	5.6	7.516
dnn51	3	11	0.211	10.2	0.652	10	3.103	11.6	11.321
dnn51	4	15	0.229	15	0.456	15	3.278	20	13.544
adder64	2	4	0.276	3.2	0.858	3	5.765	3	17.994
adder64	3	9	0.284	8.4	0.883	8	5.78	8.4	25.086
adder64	4	12	0.295	10.8	0.919	9	5.73	11.4	32.609
cc64	2	15	1.371	15	7.549	15	105.616	2.8	11.651
cc64	3	28	1.378	28	11.271	28	100.415	15	13.952
cc64	4	47.2	1.413	47.2	15.375	47	87.585	27	17.439
cat65	2	1	0.028	1	0.041	1	0.075	1	4.745
cat65	3	3.8	0.04	3.8	0.053	4	0.084	2	5.737
cat65	4	8	0.051	8	0.064	21	0.123	3	7.568
ising66	2	1	0.071	1	0.113	1	0.505	1	0.261
ising66	3	2	0.076	2	0.118	2	0.502	2	0.355
ising66	4	3	0.078	3	0.12	3	0.506	3	0.476
knn67	2	1	0.187	1	0.309	1	11.154	1	15.006
knn67	3	2	0.199	2	0.321	2	8.785	2	24.856
knn67	4	6	0.215	6	0.339	6	4.692	6	33.805
bv70	2	1	0.017	1	0.025	1	0.072	0	2.066
bv70	3	1	0.019	1	0.027	1	0.079	11.2	2.862
bv70	4	2	0.022	2	0.03	3	0.061	16.2	3.739
qugan71	2	5	0.346	5	0.725	5	11.392	3.8	15.323
qugan71	3	10	0.375	10	0.769	10	8.146	13.4	21.355
qugan71	4	15	0.403	15	0.794	15	9.485	16.6	28.418
wstate76	2	2	0.105	2	0.156	2	0.666	1.4	6.851
wstate76	3	4	0.115	4	0.165	4	0.687	3	8.636
wstate76	4	6	0.117	6	0.167	6	0.703	5	10.983
ghz78	2	1	0.039	1	0.057	1	0.103	1	6.587
ghz78	3	2	0.047	2	0.069	2	0.126	2	9.036
ghz78	4	3	0.047	3	0.066	3	0.114	3	11.393
swaptest83	2	1	0.258	1	0.444	1	26.224	1	24.362
swaptest83	3	2	0.277	2	0.466	2	20.204	2	35.5
swaptest83	4	6	0.294	6	0.482	6	17.082	6	59.982
ising98	2	1	0.147	1	0.241	1	1.354	1	0.412
ising98	3	2	0.156	2	0.25	2	1.369	2	0.578
ising98	4	3	0.164	3	0.258	3	1.378	3	0.76

rectly compute the gain of each neighbour. However, by iterating over the edges of the moved node, we avoid any redundant calculations, since we ignore contributions from edges which are not involved in the move. Once we have iterated over all edges, the cumulation of the delta gain contribution from each edge will give the delta gain for each node. After this, we proceed to resort the gain buckets according to these changes. Since the calculation of the delta gain contributions is somewhat involved, we dedicate Alg. 7 to describing this process. The bulk of these routines consists in retrieving and updating the hyper-edge configurations for each possible move. Asymptotically, this is efficient, since we can update the configurations and retrieve the costs in constant time, but the implementation involves retrieving and updating a number of different objects. As alluded to in the main text, in addition to storing and updating the root and receiver configurations, we also store the root and receiver *counts* objects, which track the number of nodes in each partition for the root and receiver sets, respectively. For each move, we increment the counts at the source and the destination of the move, then check whether the counts have changed from zero to non-zero or vice versa, indicating that the configuration must change too. Importantly, for each move, since nodes are either in the root or receiver sets, we need only update the root or receiver counts. Furthermore, since only the entries for the source and destination partition change, we only update these entries. For the full process, we need the edge costs for Φ , Φ' , $\tilde{\Phi}$ and $\tilde{\Phi}'$. In each case, $'$ corresponds to the node which has actually been moved, whereas $\tilde{}$ corresponds to the prospective move for which we are updating the delta gain. In this way, $\tilde{\Phi}$ corresponds to the prospective move being made *before* the actual node was moved. This means that, for each prospective move, we need to update the configuration for two assignment functions, corresponding to $\tilde{\Phi}$ and $\tilde{\Phi}'$. We already have the costs for Φ and Φ' , since Φ was already stored, and Φ' is updated and stored after the completed move was chosen.

A.2 Coarsening algorithms

Here we detail the algorithms employed for the coarsening process in the FM algorithm. Since we perform only temporal contraction, we simply

Algorithm 7: Delta-Gain Calculation

```

DeltaGainContrib( $v, e, p, c_e(\Phi), c_e(\Phi'), COSTS$ )
  Returns the change in gain from moving
  node  $v$  to partition  $p$  after  $\Phi$  is updated
  to  $\Phi'$ .
 $\Delta_e \leftarrow 0$ ;
Cfg[ $\tilde{\Phi}$ ]  $\leftarrow$  UpdateConfig( $e, v, p, \Phi$ );
Cfg[ $\tilde{\Phi}'$ ]  $\leftarrow$  UpdateConfig( $e, v, p, \Phi'$ );
 $c_e(\tilde{\Phi}) \leftarrow COSTS[Cfg[\tilde{\Phi}]]$ ;
 $c_e(\tilde{\Phi}') \leftarrow COSTS[Cfg[\tilde{\Phi}']]$ ;
 $\Delta_e \leftarrow c_e(\Phi') - c_e(\tilde{\Phi}') - c_e(\Phi') + c_e(\tilde{\Phi})$ ;
return  $\Delta_e$ ;

UpdateConfig( $e, v, p, \Phi$ ) Computes the
updated configuration for edge  $e$  when
node  $v$  is reassigned to partition  $p$ .
( $rootCounts, recCounts$ )  $\leftarrow$ 
  RetrieveCounts();
src  $\leftarrow \Phi(v)$ ;
/* If  $v$  is in the root set, we adjust
  rootCounts; if  $v$  is in the receiver
  set, we'd do recCounts. */
rootCounts[src]  $\leftarrow$  rootCounts[src] - 1;
rootCounts[p]  $\leftarrow$  rootCounts[p] + 1;
newCfg  $\leftarrow$ 
  UpdateJointConfig( $rootCounts, recCounts, src, p$ );

return newCfg;

UpdateJointConfig( $rootCounts, recCounts, src, dest$ )
  Updates the configuration per (Eq. 23)
  so that each partition entry is 1 if
  nonempty for either root or receiver set.
  Cfg  $\leftarrow$  RetrieveCfg();
if  $recCounts[src/dest] >$ 
   $0 \wedge rootCounts[src/dest] = 0$  then
  | Cfg[src/dest]  $\leftarrow$  1;
else
  | Cfg[src/dest]  $\leftarrow$  0;
return Cfg;

```

need to track which time-steps have been contracted in order to transform a coarse solution to a finer solution. After partitioning nodes in a coarsened graph, we read from the contraction path which nodes will be uncoarsened at the next level, and assign them the same partition as the parent node from which they have been uncoarsened. Alg. 8 details the window-based coarsening strategy, which coarsens nodes in a window of size w at each time-step. The window is moved along the time axis, coarsening nodes in the window at each step. We set the input to the algorithm as the number of levels, from which we calculate the window size. This allows us to restrict the number of levels to a fixed number. As mentioned briefly in Sec. 4, after nodes have been uncoarsened and refined once, we lock them in place to reduce the number of nodes which are moved at each level. This number is then proportional to $n_q w$, such that the uncoarsening acts like a moving window scanning and partitioning the nodes over time. Alg. 9 details the block-based coarsening strategy, which instead identifies blocks of contiguous nodes to coarsen into a single node. Similarly to the window method, we would like to be able to set the number of levels. This determines the number of blocks. We then coarsen the blocks one time-step per-level, such that the resulting number of levels is the number of time steps in each block. We also choose to add an extra level, which performs a full coarsening of the final blocks to a single time step. Alg. 10 details the recursive coarsening strategy, which coarsens pairs of neighbouring nodes at each time-step, such that the total number of nodes is halved at each time-step. This turns out to be the most effective strategy and is also leads to the fastest results when we don't cap the number of nodes moved per pass. We conjecture that this is because, at each level, all nodes are roughly as coarse as each other, i.e. each node "contains" roughly the same number of nodes. This means that the gains will not be skewed towards large super-nodes, thus controlling the partitioning at an appropriate level of granularity.

A.3 Spatial coarsening

While the paper explores only "temporal" coarsening, i.e., coarsening along the time axis, we briefly discuss the idea of spatial coarsening and how it could be incorporated in future work. Spa-

Algorithm 8: Window Coarsening of a Temporal Hypergraph (CoarsenWindow)

Input: $H_0 = (V_0, E_0)$: original (fine) hypergraph with time-layers $[0, \dots, depth]$;
depth: maximum time-layer index;
numLevels: number of coarsening levels
Output: A list $\{H_0, \dots, H_{end}\}$ of hypergraphs
CoarsenWindow($H_0, depth, numLevels$)
 $hList \leftarrow [H_0]$;
 $H \leftarrow H_0$;
 $window \leftarrow \lfloor depth/numLevels \rfloor$;
 $\ell \leftarrow depth$;
while $\ell > 0$ **do**
 $startLayer \leftarrow \max(0, \ell - window)$;
 for $\ell' \leftarrow \ell$ **to** $(startLayer + 1) \text{ step } -1$ **do**
 $H' \leftarrow \text{ContractTime}(H, \ell', \ell' - 1)$;
 $H \leftarrow H'$;
 $hList.append(H)$;
 $\ell \leftarrow \ell - window$;
return $hList$;

tial coarsening corresponds to coarsening gate-like edges, merging the nodes involved together. Consider first a basic graph, for which no gate grouping has occurred. Contracting a gate-like edge merges nodes from two qubits at the same time step together, such that partitioning of this node determines exactly where this gate will be performed, locally. In this way, if all gate edges are contracted, the partitioning will give us a fully local partitioning, where all gates are covered by state teleportation. For certain circuits, such as a QV, this would be a useful strategy. However, for many circuits, this would be a limitation, as we are removing the possibility of gate grouping. Alternatively, we may want to consider spatial coarsening after a full coarsening along the time axis. For example, if we have a very large circuit, with over 1000 qubits, then we still have a very large graph after coarsening along the time axis. We can reduce the problem size by performing further coarsening along the spatial axis, merging qubit nodes together. This could be a useful strategy for dealing with very large circuits, though we do not investigate this here. If

Algorithm 9: Block Coarsening of a Temporal Hypergraph (**CoarsenBlocks**)

Input: $H_0 = (V_0, E_0)$: original (fine) hypergraph with time-layers $[0, \dots, depth]$;
depth: maximum time-layer index;
numLevels: number of coarsening levels
Output: A list of hypergraphs $\{H_0, H_1, \dots, H_{numLevels-1}\}$
CoarsenBlocks($H_0, depth, numLevels$)
 $hList \leftarrow [H_0]$; // Store coarsening hierarchy
 $H \leftarrow H_0$;
 $blockSize \leftarrow numLevels$;
 $numBlocks \leftarrow \lfloor depth/blockSize \rfloor$;
 $\ell \leftarrow depth$;
while $\ell > 0$ **do**
 for $n \leftarrow 0$ **to** $numLevels$ **do**
 $n' \leftarrow \ell - n \times blockSize$;
 $H' \leftarrow \text{ContractTime}(H, n', n' - 1)$;
 $hList.append(H')$;
 $\ell \leftarrow \ell - 1$; // Update starting point for next window
return $hList$;

we are including gate grouping as well, there are certain considerations to make, since hyper-edges will extend over a number of time steps. If we want to contract nodes within a hyper-edge, we must restrict to nodes which are within the same time-step, i.e. contract the receiver node together with its corresponding root node, such that we do not mix time-steps, rather just commit to a local partitioning for that portion of the hyper-edge. If restricting to this rule, we may consider a strategy which alternates between spatial and temporal coarsening repeatedly. We leave this to future work.

A.4 Pre-computation costs

Here we briefly address the issue of pre-computation overhead. The efficiency of FM for our custom cost function is reliant on the fact that we can pre-compute the cost of all edge configurations in pre-processing. Of course, the number of configurations is exponential in the number of partitions, and so this is only feasible for less than 20 partitions. This will not be an issue for most early stage quantum networks, though

Algorithm 10: Recursive Coarsening of a Temporal Hypergraph (**CoarsenRecursive**)

Input: $H_0 = (V_0, E_0)$: original (fine) hypergraph with time-layers $[0, \dots, depth]$;
depth: maximum time-layer index
Output: A list of hypergraphs $[H_0, H_1, \dots, H_k]$
CoarsenRecursive($H_0, depth$) $H \leftarrow H_0$;
 $hList \leftarrow [H]$;
while *there is more than one time-layer in H* **do**
 $layers \leftarrow [0, \dots, depth]$;
 $pairsToMerge \leftarrow []$;
 for $i \leftarrow 1$ **to** $length(layers) - 1$ **step 2** **do**
 $src \leftarrow layers[i]$;
 $tgt \leftarrow layers[i + 1]$;
 $pairsToMerge.append((src, tgt))$;
 foreach $(src, tgt) \in pairsToMerge$ **do**
 $H \leftarrow \text{ContractTime}(H, src, tgt)$;
 $hList.append(H)$;
return $hList$;

in the future we will want algorithms that can handle this. There are a number of things that could be done to mitigate this. We may choose to omit the pre-computation, and rather store the cost of each configuration as it appears in computation, such that we need only perform the calculation once per configuration. Alternatively, we may choose to perform the partitioning *recursively*. In contrast to the recursive coarsening spoken about in the main text, recursive partitioning refers to multi-partitioning techniques where we partition a graph for a small number of partitions, then continue to partition the resulting subgraphs until we reach the desired number of partitions. This is also a common technique in many large-scale graph partitioning algorithms, and is something we plan to investigate in the future.